

Satellite characterization of urban aerosols: Importance of including hygroscopicity and mixing state in the retrieval algorithms

Jun Wang¹ and Scot T. Martin¹

Received 27 September 2006; revised 5 April 2007; accepted 2 May 2007; published 11 September 2007.

[1] This model study examines the sensitivity of the calculated optical properties of urban aerosols to (1) hygroscopicity and (2) internal or external mixing state, and it further investigates the associated implications for the accuracy of satellite retrievals of aerosol optical thickness (τ) and aerosol effective radius (r_{eff}). State-of-the-art retrieval algorithms widely omit variable hygroscopicity and mixing state. For the study described herein, the modeled urban aerosols are composed of water-soluble sulfates and water-insoluble black carbon (BC) in the fine mode and of water-insoluble compounds in the coarse mode. The calculations show that external compared to internal mixing of black carbon and sulfate not only significantly affects the single-scattering albedo but also alters the diagnostic relationship of the Angstrom exponent (α) to the aerosol effective radius. The implication is that over a dark surface of visible reflectance less than 0.1, satellite retrievals of urban aerosols having a BC/sulfate mass ratio of 5% can differ in τ and r_{eff} by as much as 60% and $0.2 \mu\text{m}$, respectively, depending upon the retrieval algorithm's assumptions regarding hygroscopicity and mixing state. For surface reflectances greater than 0.1 or BC/sulfate mass ratios larger than 5%, the retrieval bias, including the possibility of unphysical retrievals, increases further. The calculations also show that hygroscopic growth at elevated relative humidity increases the single-scattering albedo of urban aerosols, decreases their backscattering, and as a consequence reduces the influence of mixing state on τ and r_{eff} . These results suggest that current operational retrieval algorithms lead to a possibly systematic underestimate of aerosol optical thickness when ambient BC/sulfate aerosols are internally mixed at mass ratios greater than 3%. This study's recommendation is that aerosol retrieval algorithms, when applied to urban aerosols, incorporate in situ knowledge of relative humidity, mixing state, and BC/sulfate mass ratios, either from ground-based measurements or by auxiliary use of chemical transport models.

Citation: Wang, J., and S. T. Martin (2007), Satellite characterization of urban aerosols: Importance of including hygroscopicity and mixing state in the retrieval algorithms, *J. Geophys. Res.*, 112, D17203, doi:10.1029/2006JD008078.

1. Introduction

[2] Great progress has been made in recent years in the use of satellite sensors for the quantitative characterization of aerosol optical properties [King *et al.*, 1999; Kaufman *et al.*, 2002]. Aerosol optical thickness (τ) and aerosol effective radius (r_{eff}) are two commonly retrieved properties. Aerosol optical thickness in the visible spectrum has been retrieved over the ocean by using radiance data collected from one channel of the Advanced Very High Resolution Radiometer (AVHRR) [Rao *et al.*, 1989; Wagener *et al.*, 1997], two channels of AVHRR [Higurashi and Nakajima, 1999; Mishchenko *et al.*, 1999], and two channels of the Visible and Infrared Scanner (VIRS) [Ignatov and Stowe, 2000]. In an advance allowing higher temporal resolution

(e.g., hourly or half-hourly), data from geostationary satellites have been used to retrieve aerosol optical thickness over the ocean near the Saharan desert [Moulin *et al.*, 1997], Puerto Rico [Wang *et al.*, 2003a], and East Asia [Wang *et al.*, 2003b]. Most recently, multispectral radiance data from the Moderate Resolution Imaging Spectrometer (MODIS) [Remer *et al.*, 2005] and from the Multiangle Imaging Spectro-Radiometer (MISR) [Kahn *et al.*, 2005a], as well as polarization data from the Polarization and Directionality of the Earth's Reflectances (POLDER) satellite [Deuze *et al.*, 1999], have been used over ocean and land to retrieve both τ and r_{eff} .

[3] In the conversion of satellite-collected radiance data to aerosol optical properties (i.e., retrieval algorithms), there are recognized uncertainties that can affect the reported values of τ and r_{eff} [Abdou *et al.*, 2005]. The uncertainties stem both from simplifying assumptions used in the retrieval algorithms and from deviations of real physical processes and properties from modeled behavior. Acknowledged sources of uncertainty include, for example, the character-

¹Division of Engineering and Applied Sciences, Harvard University, Cambridge, Massachusetts, USA.

Table 1. Dry Aerosol Properties Used in This Study^a

| Aerosol Component | r_g , μm | σ_g | r_{eff} , μm | Density, g cm^{-3} | Refractive Index (at 0.55 μm) | Refractive Index (at 0.67 μm) |
|---|--------------------------|------------|------------------------------|--------------------------------|--|--|
| Externally mixed black carbon (BC) | 0.01 | 1.8 | 0.02 | 1.0 | $1.76 - 4.6 \times 10^{-1} i$ | $1.76 - 4.6 \times 10^{-1} i$ |
| Externally mixed sulfate | 0.07 | 1.8 | 0.17 | 1.7 | $1.54 - 1.0 \times 10^{-7} i$ | $1.52 - 1.0 \times 10^{-7} i$ |
| Internally mixed black-carbon/sulfate | 0.07γ | 1.8 | equation (12) | Appendix B | sulfate shell and BC core | sulfate shell and BC core |
| Externally mixed water insoluble (INSO) | 0.47 | 2.5 | 3.83 | 2.0 | $1.53 - 8.0 \times 10^{-3} i$ | $1.53 - 8.0 \times 10^{-3} i$ |

^aThe entries are mainly based upon *Hess et al.* [1998]. The density of BC is from *Lesins et al.* [2002]. See equations (1) and (2) in the text for the definitions of r_g , σ_g , and r_{eff} . See Appendix B for the definition of γ .

ization of surface reflectance [*Remer et al.*, 2005], the classification of aerosols and clouds [*Kaufman et al.*, 2005], and the calibration of satellite sensors [*Wang et al.*, 2003a; *Kahn et al.*, 2005b]. Also important in the radiative transfer model are the treatment of polarization [*Levy et al.*, 2004], aerosol multiple scattering [*Zhang et al.*, 2007], and aerosol vertical distribution [*Wang et al.*, 2003a].

[4] There has recently been an increased use of satellite-derived aerosol products for the study of urban particulate matter (PM) [*Wang and Christopher*, 2003; *Chu et al.*, 2003; *Liu et al.*, 2004; *Engel-Cox et al.*, 2004; *Al-Saadi et al.*, 2005]. These studies acknowledge that the uncertainties regarding the accuracy of the retrievals, as specifically related to urban aerosols, are in need of systematic investigation. In particular, two factors unaddressed in the current databases of urban-aerosol optical properties, as used in satellite retrievals, are aerosol hygroscopicity and internal or external mixing of the aerosol components. The present study assesses how hygroscopicity and mixing state could affect the accuracy of satellite retrievals of τ and r_{eff} of urban aerosols.

[5] The optical properties of hygroscopic aerosols, as implemented in many retrieval algorithms, correspond to a fixed relative humidity (RH) (e.g., 70% RH) [*Ferrare et al.*, 1990; *Wong and Li*, 2002]. This treatment is obviously insufficient to describe the large variation of ambient RH, even the more so in the boundary layer where urban aerosols are often located and relative humidity has high spatial and temporal variability. In the case of nonurban aerosols, the omission of RH treatment has already been shown to have quantitatively important consequences: *Kaufman et al.* [2005] showed that sea salt aerosol hygroscopicity could contribute an uncertainty of up to 0.02 to the monthly averaged τ retrieved from MODIS radiance data over ocean. *Wong and Li* [2002] showed that the disregard of smoke aerosol hygroscopicity results in retrieval errors of τ by up to 20% to 40% over boreal land. Compared to these earlier studies, the sulfate particles commonly enriched in urban aerosols imply possibly greater retrieval errors because of high sulfate hygroscopicity and great variability in boundary layer RH.

[6] The aerosol optical property databases used in state-of-the-art retrieval algorithms omit the possibilities of internal compared to external mixing of the aerosols [*Remer et al.*, 2005; *Martonchik et al.*, 1998]. Rather, in the development of the databases, external mixing was assumed [*Shettle and Fenn*, 1979; *Hess et al.*, 1998]. Urban aerosol was composed of several typical groups, such as water soluble sulfate particles, black carbon, or water-insoluble compounds (hereafter INSO) [*Hess et al.*, 1998]. In contrast, observations have shown that sulfate is commonly

internally mixed with BC and that this fine-mode aerosol mixture, combined with a nonhygroscopic coarse-mode INSO particles, is typical of urban aerosols [*Castanho et al.*, 2005; *Johnson et al.*, 2005; *Schwarz et al.*, 2006].

[7] In the study results described herein, the effects of hygroscopicity and internal or external mixing on the optical properties of typical urban aerosols (cf. Table 1) are investigated, and the associated implications for satellite retrievals of τ and r_{eff} are considered. The study strategy is to consider (1) an externally mixed aerosol at 0% RH as a base case, (2) an externally mixed aerosol at 70% RH as representative of the assumptions in retrieval algorithms [see *Ferrare et al.*, 1990; *Wong and Li*, 2002], (3) an externally mixed aerosol at variable RH for comparison to the results of parts 1 and 2 as an assessment of the effects of aerosol hygroscopicity, and (4) an internally mixed aerosol at variable RH for comparison of the results of part 3 as an assessment of the impact of mixing. Section 2 describes the methodologies used to compute optical properties and to examine satellite retrievals of τ and r_{eff} . Results and discussion are provided in section 3, and conclusions are presented in section 4.

2. Methodology

2.1. Size Distribution of Dry Aerosols

[8] A lognormal number size distribution is employed for each component j of the urban aerosol described in Table 1 [*Hess et al.*, 1998]:

$$n_j(r) = \frac{N_j}{r \ln \sigma_{g,j} \sqrt{2\pi}} \exp\left(-\frac{(\ln r - \ln r_{g,j})^2}{2 \ln^2 \sigma_{g,j}}\right) \quad (1)$$

where r_g is the geometric mean radius, σ_g is the geometric standard deviation of particle radii, N is the number of particles per unit air volume, and $n(r)$ is the number of particles having a radius between r and $r + dr$ per unit air volume. The effective radius (r_{eff}) of the number size distribution (equation (2)) is approximately predictive of the aerosol optical properties (i.e., extinction coefficient; see section 2.3) [*Hansen and Travis*, 1974]:

$$r_{eff,j} \equiv \frac{\int_{r_{\min}}^{r_{\max}} n_j(r) r^3 dr}{\int_{r_{\min}}^{r_{\max}} n_j(r) r^2 dr} \quad (2)$$

In our calculation, we set r_{\min} to 0.001 μm and r_{\max} to 20 μm . The values of r_g , σ_g , and r_{eff} of BC, sulfate, and INSO particles are given in Table 1. As an example, a typical urban aerosol is 60% by mass sulfate, 5% black carbon, and 35% INSO [*Hess et al.*, 1998]. The respective

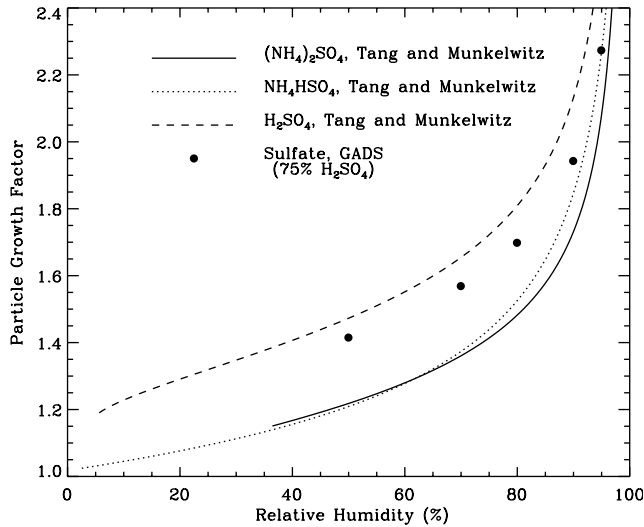


Figure 1. Particle growth factor g as a function of RH for aqueous ammonium sulfate, ammonium bisulfate, and sulfuric acid. Data are from *Tang and Munkelwitz* [1994]. Circles are the growth factors of sulfate aerosols (75% H₂SO₄) in the Global Aerosol Data Set (GADS) [*d'Almeida et al.*, 1991]. Unless stated otherwise, the growth curve of ammonium sulfate is employed in this study (i.e., Figures 2 to 10).

corresponding fractional number concentrations are 0.021, 0.979, and 3.5×10^{-6} .

2.2. Hygroscopicity of Sulfate Aerosols

[9] As RH increases, sulfate particles take up water and swell, affecting both particle diameter and refractive index. The extent of growth is a function of RH, chemical composition, and the RH history of the particles [*Martin*, 2000]. In the present study, the particle growth behavior is specified by using the growth factor $g(\text{RH})$, which is defined as the ratio of wet particle radius to the dry particle radius [*Tang*, 1996].

[10] Our treatment computes the particle growth factor as the volume-fraction weighted average of pure components [*Hanel*, 1976]. The pure components we consider are aqueous ammonium sulfate (fully neutralized), aqueous ammonium bisulfate (half neutralized), and sulfuric acid (no neutralization) [*Tang and Munkelwitz*, 1994; *Tang*, 1996]. Figure 1 shows that the growth factor used for sulfate aerosols in the traditional aerosol optical databases [*d'Almeida et al.*, 1991] is not accurate between 5% and 85% RH for describing the hygroscopic growth of partially neutralized sulfate particles. The dependence on the extent of neutralization, however, is less than on aerosol hygroscopicity and on internal or external mixing: the variation of single scattering albedo and the phase function due to composition differences is less than 15% for a fixed RH and mixing state [*Tang*, 1996]. For this reason, the results described in this study are restricted to ammonium sulfate, which is more representative than sulfuric acid of boundary-layer compositions nearby to urban centers [*Martin et al.*, 2004]. In contrast, optical properties of sulfuric acid are assumed in the database widely employed in satellite retrievals, even for urban aerosols [*d'Almeida et al.*, 1991].

[11] The function $g(\text{RH})$ of ammonium sulfate is potentially complicated by phase transitions. Dry ammonium sulfate particles start to grow only at 80% RH, which is called the deliquescence RH (DRH). As RH decreases, aqueous ammonium sulfate particles start to shrink and become solid at 35% RH, a point referred to as the crystallization RH (CRH). This hysteresis between DRH and CRH has important ramifications for quantifying aerosol radiative forcing [*Martin et al.*, 2004]. The focus of the present analysis, however, is restricted to the upper branch of the hysteresis loop [e.g., *Nemesure et al.*, 1995]. This restriction also implies that the shape of the particles is spherical.

[12] The wet sulfate particle size distribution $n^{\text{wet}}(r')$ can be written in terms of the dry distribution $n^{\text{dry}}(r)$ as follows:

$$n^{\text{wet}}(r')dr' = n^{\text{dry}}(r)dr \quad \text{where } r' = gr \quad (3)$$

under the assumption that the number of particles does not change during the hygroscopic growth (e.g., as possibly by coagulation or deposition). Hence the wet particle size distribution has a lognormal form similar to that of the dry particle size distribution, although r_g is scaled by a factor of $g(\text{RH})$ [*Li et al.*, 2001].

2.3. Optical Properties of One Aerosol Type

[13] The extinction coefficient K_j^{ext} and the scattering coefficient K_j^{sca} of an aerosol of type j (i.e., sulfate, BC, or INSO) having a size distribution $n_j(r)$ are computed at wavelength λ as follows [*Hess et al.*, 1998]:

$$K_j^{\text{ext}}(\lambda) = \int_{r_{\text{min}}}^{r_{\text{max}}} Q_j^{\text{ext}}(r, m_j, \lambda) \pi r^2 n_j(r) dr \quad (4)$$

$$K_j^{\text{sca}}(\lambda) = \int_{r_{\text{min}}}^{r_{\text{max}}} Q_j^{\text{sca}}(r, m_j, \lambda) \pi r^2 n_j(r) dr \quad (5)$$

where Q_j^{ext} and Q_j^{sca} are, respectively, the extinction and scattering efficiencies of individual particles (e.g., obtained from Lorenz-Mie theory for spherical particles) having refractive indices $m_j(\lambda)$. The single-scattering albedo ω_j and the phase function $P_j(\theta)$ of the aerosol are computed as follows:

$$\omega_j(\lambda) = \frac{K_j^{\text{sca}}(\lambda)}{K_j^{\text{ext}}(\lambda)} \quad (6)$$

$$P_j(\theta, \lambda) = \frac{\int_{r_{\text{min}}}^{r_{\text{max}}} Q_j^{\text{sca}}(r, m_j, \lambda) \pi r^2 n_j(r) p(\theta, r, m_j, \lambda) dr}{K_j^{\text{sca}}(\lambda)} \quad (7)$$

where $p(\theta)$ is the single-particle phase function at scattering angle θ , which is normalized by 4π in our treatment [*Hess et al.*, 1998].

[14] Equations (4) to (7) show that the aerosol optical properties depend on the number size distribution, the shape, and the refractive index of the constituent particles. These parameters depend on aerosol dry chemical composition and ambient meteorological conditions, such as

relative humidity [d'Almeida *et al.*, 1991]. The absorption of water, which is especially important for sulfate aerosols, both increases the particle size and alters the refractive index [Hanel, 1976]. There are two common methods to calculate the effective refractive index of an aerosol particle having a homogenous mixed composition. The first is based upon the volume mixing of each component [Hanel, 1976], and the second is based on the molar refraction of each component [Moelwyn-Hughes, 1961]. The two methods yield negligible differences for partially to wholly neutralized sulfate (cf. Appendix A), and the molar-refraction method is employed in the current study.

2.4. Optical Properties of Externally Mixed Aerosol Types

[15] For externally mixed aerosols, the particles of the different aerosol types sulfate, BC, and INSO are entirely physically separate. The overall optical properties are then the sum of those of the component aerosols, as follows [e.g., Hess *et al.*, 1998]:

$$K^{ext}(\lambda) = \sum K_j^{ext}(\lambda) \quad (8)$$

$$K^{sca}(\lambda) = \sum K_j^{sca}(\lambda) \quad (9)$$

$$\omega(\lambda) = \frac{K^{sca}(\lambda)}{K^{ext}(\lambda)} \quad (10)$$

$$P(\theta, \lambda) = \frac{\sum K_j^{sca}(\lambda) P_j(\theta, \lambda)}{K^{sca}(\lambda)} \quad (11)$$

$$r_{eff} = \frac{\sum n_j(r) r^3 dr}{\sum n_j(r) r^2 dr} \quad (12)$$

$$\alpha = \frac{\ln K^{ext}(\lambda_2) - \ln K^{ext}(\lambda_1)}{\ln \lambda_1 - \ln \lambda_2} \quad (13)$$

for $j \in \{\text{sulfate, BC, INSO}\}$.

[16] An α value, representing the wavelength dependence of K^{ext} , is a good indicator of aerosol effective radius: for typical atmospheric particles at solar wavelengths a larger value of α corresponds to a smaller r_{eff} because the wavelength dependence of $Q^{ext}(\lambda)$ increases for smaller size parameter $2\pi r/\lambda$ [Tomasi *et al.*, 1983]. Thus for the larger r_{eff} , the relative change of Q^{ext} and K^{ext} (cf. equation (4)) with λ is smaller. The aerosol Angstrom exponent α in this study is calculated for $\lambda_1 = 0.55 \mu\text{m}$ and $\lambda_2 = 0.67 \mu\text{m}$. For typical urban aerosols, Eck *et al.* [1999, Figure 8] show that an α value calculated at 0.55 and 0.67 μm provides a good representation of the overall wavelength dependence from 0.34 to 1.02 μm .

2.5. Optical Properties of Internally Mixed Aerosol Types

[17] For the internally mixed treatment, BC and sulfate occur in the same particle in the fine mode while INSO particles remain externally mixed from them in the coarse mode. The overall optical properties are therefore calculated

in two steps. First, Q^{ext} , Q^{sca} , and p of the internally mixed BC/sulfate particles are computed (vida infra), from which K^{ext} , K^{sca} , ω , and P are determined by equations (4) to (7). Second, the overall optical properties of the externally mixed aerosol are obtained by using equations (8) to (13) for $j \in \{\text{mixed BC/sulfate, INSO}\}$. As a caveat, although coarse-mode INSO particles can also become coated by sulfate during long-range transport, these coatings, unlike their counterparts on BC particles, are not optically important because they result in relatively small changes of particle size and refractive index.

[18] Two approaches have been used in previous studies to calculate the optical properties of internally mixed BC/sulfate particles [Lesins *et al.*, 2002]. (1) A refractive index is calculated by assuming that sulfate and BC are homogeneously mixed (cf. Appendix A). The derived refractive index and the particle size are then used in a Lorenz-Mie calculation of Q^{sca} , Q^{ext} , and p . (2) A BC-core/sulfate-shell structure is assumed, and a core/shell Mie code is employed, which requires input of the refractive indices of BC and sulfate as well as the core and shell particle radii [Ackerman and Toon, 1981; Redemann *et al.*, 2001]. The difference of Q^{sca} , Q^{ext} , and p predicted by the two methods, however, is small [Lesins *et al.*, 2002], and we employ the core/shell model.

[19] In addition to these two cases, a third plausible case is that several BC particles could be randomly imbedded inside a sulfate particle, either centrally or eccentrically, because BC particles have a larger number concentration than sulfate particles in a typical urban aerosol plume. As a statistical average of a particle ensemble, however, in which BC particles are randomly positioned inside each sulfate particle, the optical properties are equivalent to those of an agglomerated BC core inside each sulfate particle [Chylek *et al.*, 1995], which corresponds to our case 2.

[20] In calculations comparing external and internal mixing, the relative mass percentage of each aerosol component is conserved (cf. Appendix B).

3. Results and Discussion

3.1. Optical Properties of Sulfate and Black-Carbon Aerosols

[21] The phase functions $P(\theta)$ of aqueous ammonium sulfate aerosols are shown in Figure 2 for several RH values and internal or external mixing with 5% by mass of BC. Elevated RH increases forward scattering (i.e., $P(\theta)$ for $\theta \rightarrow 0^\circ$) because particle growth enhances forward diffraction [Liou, 2002]. Likewise, backscattering at 180° weakens for elevated RH, decreasing by 45% for 90% RH compared to 0% RH (Figure 2a inset). The average decrease across all backscattering angles (i.e., $90^\circ < \theta < 180^\circ$) is 60%.

[22] The effect of hygroscopicity on sulfate aerosol backscattering can be compared to the effect of nonsphericity on dust aerosol backscattering. The latter effect increases $P(\theta)$ for $\theta < 150^\circ$ but decreases it for $\theta > 150^\circ$ [Wang *et al.*, 2003c]. In comparison, sulfate hygroscopicity decreases $P(\theta)$ for all backscattering angles (Figure 2a). The magnitude of the variation in $P(\theta)$ is nearly the same for both effects. Therefore in satellite retrieval algorithms for τ that employ angular-dependant radiance observations, the possibility of aerosol hygroscopicity should be considered.

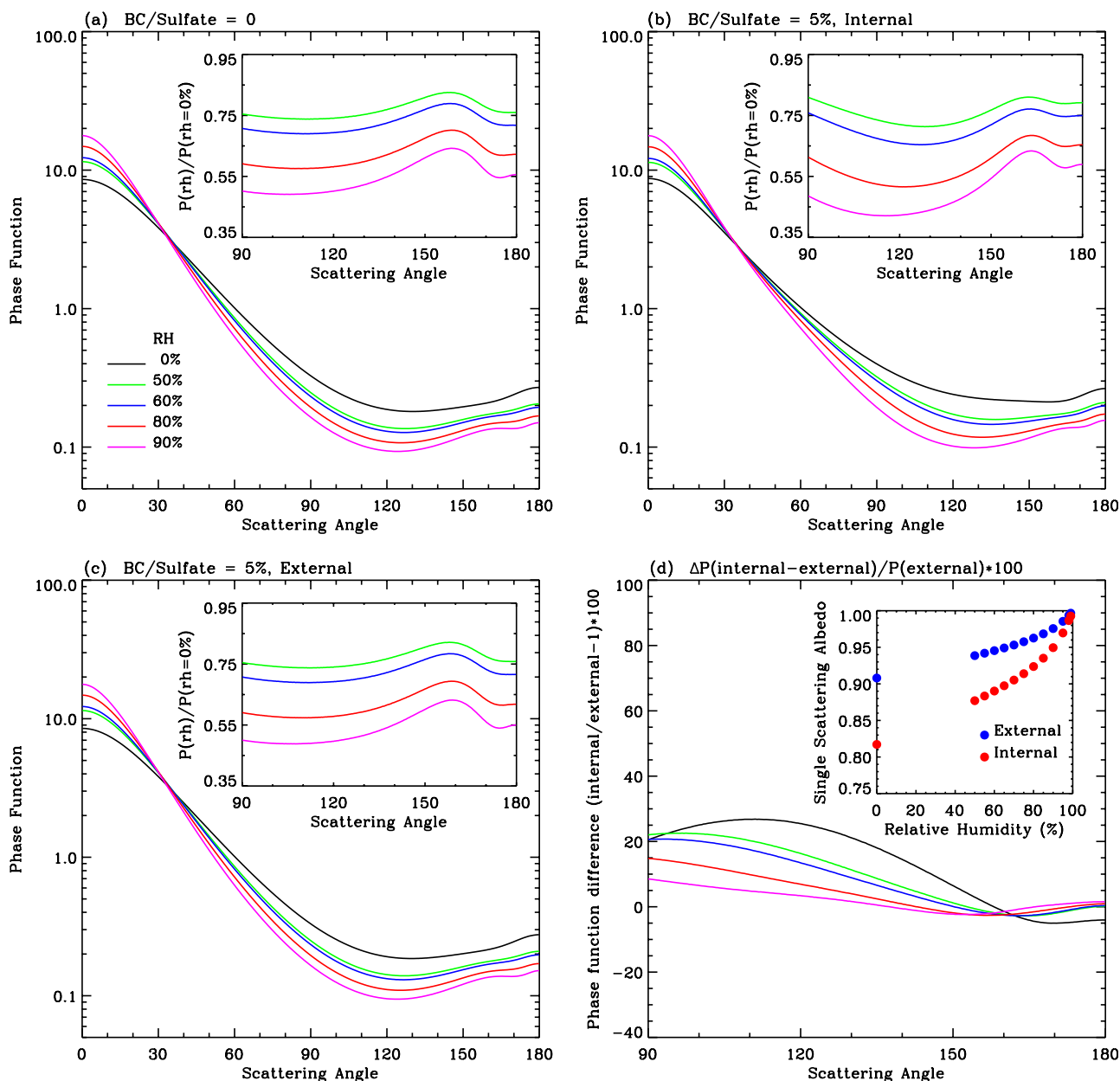


Figure 2. (a) Phase function at $0.67 \mu\text{m}$ of aqueous ammonium sulfate particles for different relative humidities. (b, c) Same as Figure 2a except that there is 5% by mass black carbon internally and externally mixed, respectively, with sulfate. The insets in Figures 2a, 2b, and 2c show the ratio of the phase function at elevated RH to that at 0% RH (excluding aerosol hygroscopicity). (d) The percentage difference of the phase function for external compared to internal mixing. The inset shows the single-scattering albedo. Aerosol parameters are given in Table 1. INSO particles are not included in the calculations shown for this figure.

[23] The effects of aerosol mixing on the phase functions can be seen by comparing Figures 2b and 2c (internal and external mixing, respectively) with Figure 2a (sulfate alone). The phase functions corresponding to aqueous sulfate particles internally mixed with 5% by mass of BC at several RH values (Figure 2b) are broadly similar to those of sulfate alone (Figure 2a). However, a detailed comparison afforded by the insets in Figures 2a and 2b shows that above 80% RH internal mixing with BC significantly decreases $P(\text{RH})/P(\text{RH} = 0)$ for $90^\circ < \theta < 160^\circ$ RH. The conclusion is that the internal mixing of BC with sulfate

amplifies the decrease of backscattering caused by hygroscopic growth. In contrast, external mixing of sulfate and BC aerosols (Figure 2c) leaves $P(\theta)$ nearly unchanged compared to sulfate alone, a result explained by the small scattering coefficient of externally mixed BC particles because of their small size. There is also an absolute increase of $P(\theta)$ for internal compared to external mixing, which is greatest for lower RH (Figure 2d). The maximum difference is 25% at $\theta = 120^\circ$ and 0% RH.

[24] The mixing state also has an important effect on the single-scattering albedo (Figure 2d inset). The ω value of

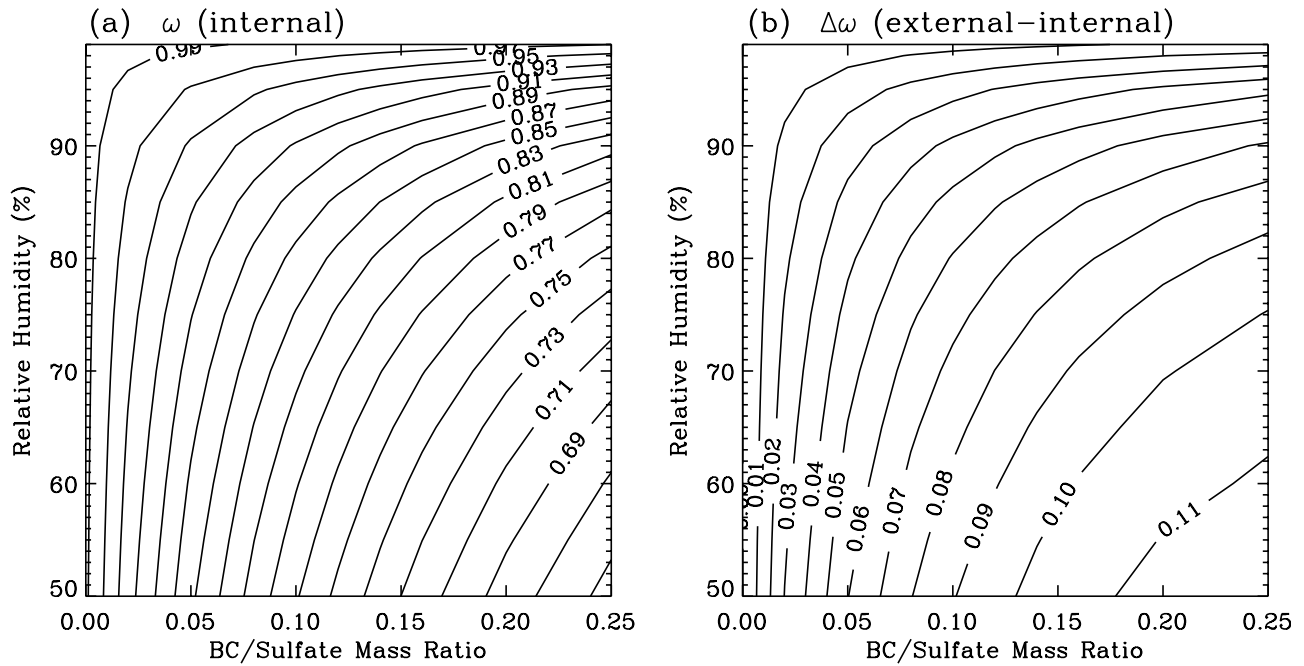


Figure 3. (a) Isopleths of single-scattering albedo (ω) for variable RH and BC/sulfate mass ratio for internal mixing. (b) Isopleths for the difference in the single-scattering albedo ($\Delta\omega$) for external compared to internal mixing. Aerosol properties are given in Table 1. INSO particles are not included in the calculations shown in this figure.

internal mixing is 0.08 smaller than that of external mixing at 0% RH because the BC core enhances the light absorption inside the sulfate shell [Ackerman and Toon, 1981]. The enhancement, however, weakens as the shell radius increases for a fixed core radius. The difference of ω caused by the aerosol mixing state therefore decreases because of hygroscopic growth at elevated RH, approaching zero for $\text{RH} > 95\%$.

[25] Isopleths of ω for variable RH and BC/sulfate mass ratio are shown in Figure 3a for internal mixing. As expected, higher BC/sulfate mass ratios and lower RH values favor smaller ω values. In addition, hygroscopic growth (i.e., an RH dependence to the isopleths) affects ω for mass ratios greater than 0.05. The mass ratio has its most significant effect on ω for $\text{RH} < 90\%$. For higher RH, increasing the mass ratio has a small effect because the enhancement of light absorption by BC saturates for large particles (i.e., hygroscopic growth, as described for inset of Figure 2d). Isopleths for the difference of ω between internal and external mixing are shown in Figure 3b. Internal mixing decreases ω by 0.01 to 0.11, with the greatest effect at low RH and high BC/sulfate mass ratio. The role of INSO particles was also explored (results not shown), but due to their smaller number concentrations, the external mixing of INSO with sulfate and BC had a negligible effect on the overall phase function and single-scattering albedo.

3.2. Implications for Satellite Characterization of Aerosols

3.2.1. Theory Regarding Satellite Retrievals of τ and r_{eff}

[26] The theory employed in this study for the retrieval of τ and r_{eff} follows that of Wang *et al.* [2003a, 2003b]. Briefly, the satellite measures an irradiance on a pixel of

its imaging sensor (W m^{-2}) that, given the geometric and spectral factors of the instrument and the assumption of a point source, is converted to a radiance (L_{sat} , $\text{W m}^{-2} \text{sr}^{-1} \mu\text{m}^{-1}$) upwelling from the top of atmosphere. Satellite-measured reflectance ρ_{sat} is given by $\rho_{\text{sat}} = L_{\text{sat}}/L_{\text{solar}} = \pi L_{\text{sat}}/S_0\mu_0$ where L_{solar} is the collimated solar radiance incident at the top of atmosphere, S_0 is the solar constant, and μ_0 is the cosine of solar zenith angle [Higurashi and Nakajima, 1999]. An expected value of the radiance at the top of atmosphere ($L_{\text{model_toa}}$) and hence the reflectance ($\rho_{\text{model_toa}} = L_{\text{model_toa}}/L_{\text{solar}}$) at a given relative sun-sensor positioning can be calculated under cloud-free conditions by using a radiative transfer model (RTM) that considers the radiation source strength (i.e., the Sun), atmospheric scattering and absorption by gas molecules and aerosol particles, and the Earth's surface reflectance (ρ_{sfc}).

[27] When the other parameters are known, the essence of the satellite aerosol retrieval algorithm is to invoke a set of physically consistent aerosol optical properties in the model (thereby implying values of τ and r_{eff}) that minimize the difference quantity $\rho_{\text{sat}} - \rho_{\text{model_toa}}$. Consequently, the retrieval accuracies of τ and r_{eff} are susceptible to the uncertainties in the selected aerosol optical properties, in addition to other uncertainties such as in estimating ρ_{sfc} and in measuring ρ_{sat} (i.e., the sensor calibration). To better identify the effects of uncertainties in aerosol optical properties, we assume in the following analysis that there are no errors in ρ_{sfc} and ρ_{sat} and that the properties of the Sun and the atmospheric gases are accurately known.

3.2.1.1. Retrieval of τ

[28] In this study, we employ the plane-parallel discrete-ordinate scalar radiative transfer model DISORT [Stamnes *et al.*, 1988; Ricchiazzi *et al.*, 1998; Wang *et al.*, 2003a] to compute the upwelling radiance $L_{\text{model_toa}}$, thus inferring

ρ_{model_toa} . The calculations are systematically completed for different surface reflectances and Sun-sensor relative positions μ and φ , where μ is the satellite-viewing zenith angle of $\cos^{-1}(\mu)$ and φ is the relative Sun-satellite azimuth angle. Absorption and Rayleigh scattering by atmospheric gases are considered for a tropical summer atmospheric profile [McClatchey *et al.*, 1971]. Aerosol optical properties K^{ext} , ω , and $P(\theta)$ used in the calculation are varied for the cases described in section 2 for different BC/sulfate mixing states, relative humidity values, and mass ratios among BC, sulfate, and INSO. Different τ values, calculated as K^{ext} multiplied by 3 km for the assumption that aerosols are evenly distributed in a 3-km planetary boundary layer, are explored by increasing the total aerosol loading (i.e., adjusting N in equation (1) and thus K^{ext} in equations (4) and (5)). This set of calculations provides a set of values that can be arranged as a function lookup table for ρ_{model_toa} having eight input parameters, namely τ , ρ_{sfc} , μ , μ_0 , φ , RH, aerosol mixing state, and dry BC/sulfate/INSO mass ratio. Provided that the other seven input parameters are known, a retrieval of τ from an observation of ρ_{sat} is accomplished by varying τ until ρ_{model_toa} matches ρ_{sat} . A satellite observation, however, provides only three input parameters, namely μ , μ_0 , and φ . Therefore a unique retrieval of τ is not possible without assumptions for the remaining input parameters, including ρ_{sfc} , RH, aerosol mixing state, and dry BC/sulfate/INSO mass ratios. We investigate in section 3.2.2 how different assumed values of these parameters affect the retrieval of τ .

3.2.1.2. Retrieval of r_{eff}

[29] In regard to the retrieval of r_{eff} , there are various approaches, all based upon the use of multispectral reflectance data, to infer information about the aerosol size. Examples include the retrieval of the aerosol Angstrom exponent α [Higurashi and Nakajima, 1999; Mishchenko *et al.*, 1999], the retrieval of the fine-mode fractional contribution to τ [Tanre *et al.*, 1997], and the retrieval of the aerosol effective radius r_{eff} [Martonchik *et al.*, 1998]. Although these methods differ in the retrieved parameters, they have in common the use of the physical principle that the aerosol Angstrom exponent α is sensitive to the aerosol number size distribution [Tomasi *et al.*, 1983; Wang *et al.*, 2003b]:

$$\alpha = \frac{\ln \tau(\lambda_2) - \ln \tau(\lambda_1)}{\ln \lambda_1 - \ln \lambda_2} = \dots = \frac{\ln K^{ext}(\lambda_2) - \ln K^{ext}(\lambda_1)}{\ln \lambda_1 - \ln \lambda_2} = f(r_{eff}) \quad (14)$$

where the quantity on the left-hand side (LHS) is calculated based upon satellite observations (e.g., as described in section 3.2.1.1) and the relationship on the right-hand side (RHS) is established by the optical properties database (e.g., through use of equations (12) and (13)).

[30] Use of equation (14) in the interpretation of satellite observations requires that the optical properties database of the RHS be uniquely established so that $\alpha = f(r_{eff})$ can be inverted to $r_{eff} = h(\alpha)$. This second relationship allows satellite measurements of the aerosol Angstrom exponent to be used to retrieve r_{eff} . For this unique inversion to be possible, however, an important assumption imbedded in typical retrieval algorithms is that each aerosol type has having a known wavelength-dependent refractive index and a known lognormal size distribution of fixed r_g and

σ_g (cf. equation (1)), and the variation of r_{eff} in the atmosphere is primarily caused by the change of number mixing ratio among different types of aerosols. Some retrieval algorithms alternatively employ ground- or air-based in situ measurements of size distributions and optical properties of aerosols to calibrate $r_{eff} = h(\alpha)$ for specific uses [Wang *et al.*, 2003a].

[31] In the current study, the implications of a nonunique inversion for urban aerosols are assessed as follows. The RHS of equation (14) is calculated from K^{ext} values at 550 and 670 nm (equation (8)) and from r_{eff} values (equation (12)) for many aerosol cases, including external and internal mixing, a range of RH values, and a range of mass ratios between the fine (i.e., BC and sulfate) and coarse (i.e., INSO) particles. Because the LHS equals the RHS of equation (14), the results of these forward modeling calculations serve as an inverse-modeling lookup table for the relationship between α and r_{eff} , effectively providing a functional relationship of $r_{eff} = h(\alpha; \text{mixing state, RH, mass ratio})$. This function collapses to a unique relationship of $r_{eff} = h(\alpha)$ only in the special case that two of three parameters (i.e., mixing state, RH, or mass ratio) have fixed, known values. The calculated relationships between α and r_{eff} are shown in Figures 8 to 10 and discussed in detail in section 3.2.3.

3.2.2. Uncertainties in Aerosol Optical Thickness

[32] Figure 4 shows several cross cuts of the dependence of ρ_{model_toa} on τ . Figures 4a–4e show different surface reflectances and BC/sulfate mass ratios, with the lines showing different relative humidities. Internal mixing of BC and sulfate is assumed. For low ρ_{sfc} values (such as 0.06 in Figures 4a, 4b, and 4c) and small τ values, ρ_{model_toa} and τ are positively linearly correlated, which can be explained by equation (15) valid for the single-scattering regime and for low surface reflectance [Wagner *et al.*, 1997; Higurashi and Nakajima, 1999]:

$$\rho_{model_toa} = \rho_{sfc} + \rho_{mol} + \frac{\omega P(\theta)}{4\mu\mu_0} \tau \quad (15)$$

where $\cos\theta = \mu\mu_0 + (1 - \mu^2)^{0.5}(1 - \mu_0^2)^{0.5} \cos\varphi$ and ρ_{mol} is the reflectance from molecular absorption and scattering (typically between 0.01 and 0.05) [Wagner *et al.*, 1997]. In the absence of BC (Figure 4a; $\omega \rightarrow 1$), ρ_{model_toa} decreases for fixed τ as RH increases as a consequence of the decreased backscattering of the larger particles present at elevated RH (Figure 2a). As the BC/sulfate mass ratio increases to 5%, however, ρ_{model_toa} drops markedly at low RH, and as a result ρ_{model_toa} values at low and high RH are virtually equal (Figure 4b). The explanation is a balance between the smaller ω but greater backscattering for low RH than for high RH (cf. Figures 2b and 2d). For even greater BC/sulfate mass ratio (e.g., mass ratio of 18% in Figure 4c), the balance shifts further in the favor of even smaller ω , and as a result, ρ_{model_toa} increases for fixed τ as RH increases. Figures 4a and 4c thus represent reverse trends depending on the BC/sulfate mass ratio.

[33] For high τ values (i.e., the single-scattering approximation fails) and for high ρ_{sfc} , the expected breakdown in the linear relationship between ρ_{model_toa} and τ (as described by equation (15)) is apparent in Figure 4. For example, for a BC/sulfate mass ratio of 5%, Figure 4 shows that as ρ_{sfc} increases from 0.06, to 0.12, to 0.18 in Figures 4b, to 4d,

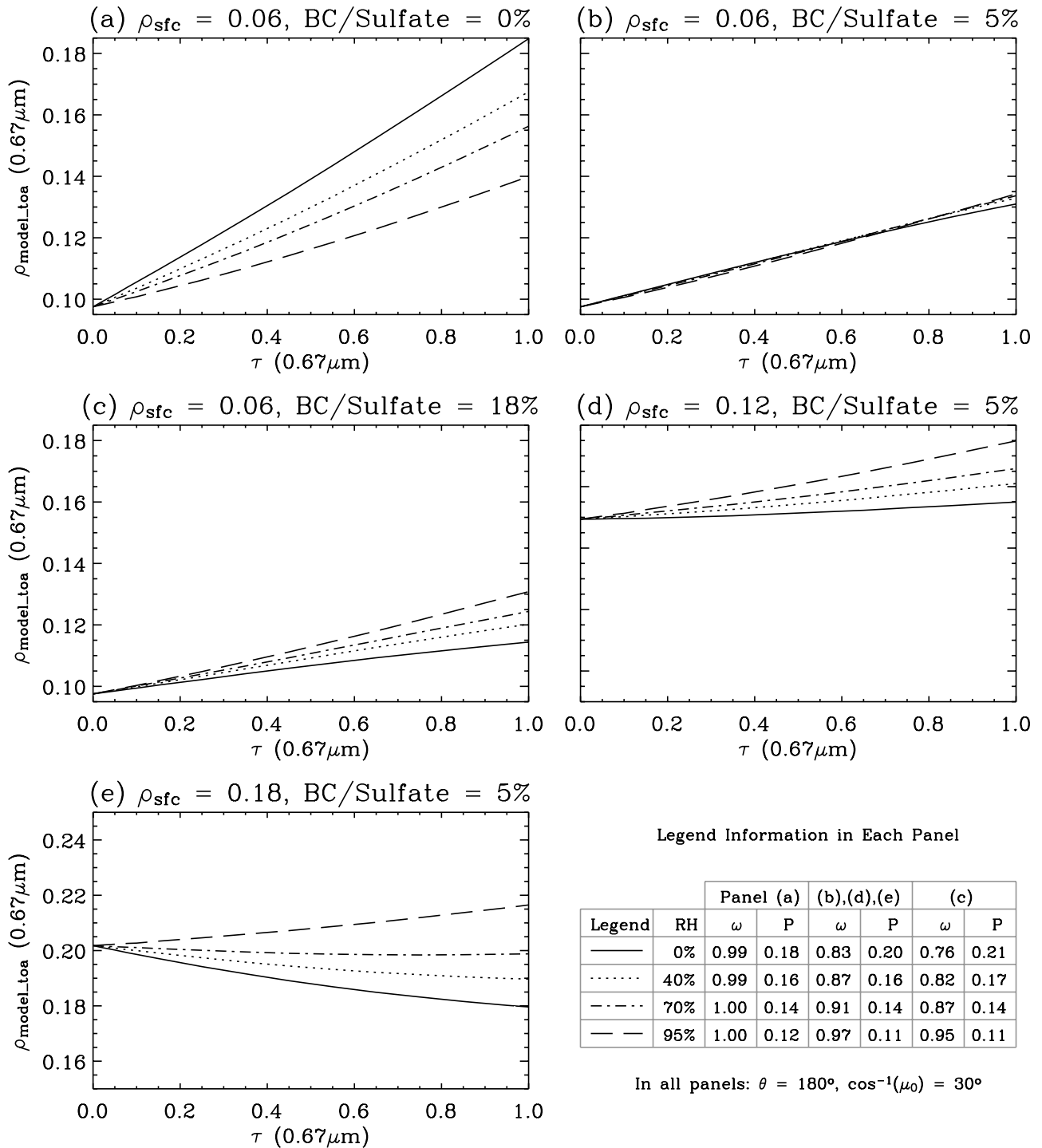


Figure 4. Relationship between modeled satellite reflectance at the top of the atmosphere (ρ_{model_toa}) and aerosol optical thickness (τ), showing (a)–(e) results for variable surface reflectances and BC/sulfate mass ratios (internally mixed). Lines show calculations at 0% (i.e., excluding aerosol hygroscopicity), 40%, 70%, and 95% RH. Aerosol properties are given in Table 1. The INSO/(BC + sulfate + INSO) ratio is 35% for the calculations shown in this figure. The difference between ρ_{model_toa} and ρ_{sfc} at $\tau = 0$ arises from Rayleigh scattering by atmospheric gases. In legend table, ω is the single scattering albedo, and P is the phase function at $\theta = 180^\circ$.

to $4e$, an increase in τ leads to a decrease in ρ_{model_toa} (i.e., the reverse of the typical case) for ρ_{sfc} of 0.18 and 40% RH and greater (Figure 4e). This negative correlation occurs when the aerosol is more absorptive than the surface (such as internally mixing BC with sulfate at low RH), and it is further favored for greater τ because multiple scattering leads to additional absorption, both for the downward and the upward solar radiation. These results imply that ρ_{sfc} should be less than 0.12 (at least for the conditions of Figure 4) in order that the magnitude of the slope between ρ_{model_toa} and τ is large enough that an observation ρ_{sat} , given its uncertainties, well constrains τ for all RH values, which is an important criterion for accurate retrievals.

[34] An analysis for the case of external mixing is similar as discussed for the results shown in Figure 4 for internal mixing except that ρ_{model_toa} is less sensitive to the BC/sulfate mass ratio because ω is larger for external compared to internal mixing (Figure 2d).

[35] Figure 4 also imparts an informative caution: the omission of an RH treatment in the retrieval algorithm can result in unphysical τ values (i.e., negative or alternatively unrealistically large). For instance, to match the value of ρ_{model_toa} to an observed ρ_{sat} value of 0.17 for the conditions of Figure 4d, a retrieval algorithm that is tuned to 5% RH when the ambient RH is actually 70% will retrieve an unphysically large τ value (i.e., $\tau \gg 1$ at 5% RH) instead of the accurate value (i.e., $\tau = 0.6$ at 70% RH). Likewise, an unphysical $\tau < 0$ will be obtained for the conditions of Figure 4e to match ρ_{model_toa} with ρ_{sat} when $\rho_{sat} = 0.21$ for ambient RH of 95% in a retrieval algorithm assuming 70% RH. These cautionary results highlight that even in cases for which positive τ is retrieved, the accuracy of τ may be in substantial error if hygroscopicity is not considered, and, alarmingly, no obvious hint of $\tau < 0$ may be apparent.

[36] With a view toward a focus on the satellite characterization of urban aerosols over dark surfaces, the remainder of the analysis in this paper is for retrievals of τ under the condition $\rho_{sfc} < 0.1$. In addition to ocean, vegetation, pasture, and forest, this restriction also encompasses urban regions that have dominant vegetation cover. The present-day MODIS aerosol retrieval algorithm, for example, is operational over land for $\rho_{sfc} < 0.125$ at $0.67 \mu\text{m}$, and dark pixels are located within urban regions [Kaufman et al., 1997; Remer et al., 2005].

[37] Figures 5 to 7 provide cross cuts of calculated τ values with different assumption about aerosol hygroscopicity and mixing state. The figures have in common a denominator of $\tau(\text{int, RH} = \text{var})$, which is taken to represent the actual state of ambient aerosols in the column (i.e., internally mixed and responsive to relative humidity) and the corresponding optical thickness. The panels in the figures then assume several different numerators (e.g., $\tau(\text{ext, RH} = \text{var})$), which are taken to represent the τ that would be retrieved by a satellite algorithm making those assumptions. RH = 0 indicates the omission of aerosol hygroscopicity in the algorithm. The error in the satellite algorithm is then the difference from unity of the ratio in the two τ values.

3.2.2.1. Effect of Hygroscopicity

[38] Isopleths of the ratio of the aerosol optical thickness without and with consideration of aerosol hygroscopicity

are shown in Figure 5 for two different cross cuts of BC/sulfate mass ratio (Figures 5a and 5b) and two different scattering angles (Figures 5c and 5d). Internal mixing is assumed. For a BC/sulfate ratio of 0% (Figure 5a), $\tau(\text{RH} = 0)/\tau(\text{RH})$ decreases from 0.85 to 0.65 as RH increases from 45% to 90%. The angular variation is less than 0.05. This RH- θ dependency is rationalized by equation (15) as a decrease of $P(\theta; \text{RH})/P(\theta; \text{RH} = 0)$ for increasing RH (cf. inset of Figure 2a), given that ω remains near unity at all RH values. As the BC/sulfate mass ratio increases, however, a gain in $\omega(\text{RH})/\omega(\text{RH} = 0)$ for elevated RH (cf. inset of Figure 2d and also Figure 3a) compensates for the decrease in $P(\theta; \text{RH})/P(\theta; \text{RH} = 0)$. As a result, for a BC/sulfate mass ratio of 5% (Figure 5b), $\tau(\text{RH} = 0)/\tau(\text{RH})$ is within 0.10 of unity for RH < 90%. Further increases in the BC/sulfate mass ratio lead to $\tau(\text{RH} = 0)/\tau(\text{RH}) > 1$ (Figure 5c), indicating that a retrieval algorithm assuming optical properties at 0% RH (i.e., omitting aerosol hygroscopicity) can overestimate the true aerosol optical thickness when the ambient RH is elevated.

[39] The magnitude of the error in the retrieved aerosol optical thickness caused by an omission of RH in the algorithm depends on the ambient RH, the BC/sulfate mass ratio, and the scattering angle of the observation. For BC/sulfate mass ratios of less than 3%, τ is underestimated by 15 to 35% depending on ambient RH, relatively independent of θ (Figure 5a). In contrast, for a BC/sulfate mass ratio of 10% and θ of 180° , the retrieved τ is overestimated by 40% at an ambient RH of 70% and by 80% at an ambient RH of 90%. For $\theta = 120^\circ$, τ can be underestimated by up to 30% or overestimated by up to 40% for ranges of 0 to 18% in BC/sulfate mass ratios and of 40 to 95% in ambient RH. For the same ambient RH and BC/sulfate ratio, $\tau(\text{RH} = 0)/\tau(\text{RH})$ values are generally larger at $\theta = 180^\circ$ than at $\theta = 120^\circ$, because a gain in $\omega(\text{RH})/\omega(\text{RH} = 0)$ for elevated RH is compensated more by the larger decrease of $P(\theta; \text{RH})/P(\theta; \text{RH} = 0)$ at $\theta = 180^\circ$ than at $\theta = 120^\circ$.

3.2.2.2. Effect of Aerosol Mixing State

[40] Figures 6 and 7 provide cross cuts showing the effects of mixing state on retrieved aerosol optical thickness. As implied by equation (15), mixing state affects the magnitude of the retrieved τ by increasing ω (Figure 3b) and decreasing $P(\theta)$ (Figure 2d) for external compared to internal mixing. The dependence of $P(\theta)$ on mixing state is nearly negligible for $\theta \rightarrow 180^\circ$ but much greater for $\theta < 140^\circ$. As a net effect of changes in $\omega P(\theta)$ (i.e., the pseudo phase function), the ratio of $\tau(\text{external})/\tau(\text{internal})$ for a BC/sulfate mass ratio of 5% is 0.80 to 0.98, depending on RH and the scattering angle (Figure 6a), showing that the increase in ω is greater than the decrease in $P(\theta)$. A retrieval algorithm assuming external mixing thus underestimates τ by 2% to 20% in the case that the ambient aerosol is internally mixed. The underestimate of 20% corresponds to lower RH values and higher scattering angles (Figure 6a). The underestimate further increases at higher BC/sulfate mass ratios. For a BC/sulfate mass ratio of 10%, for instance, the underestimate is 40% at 50% RH.

[41] Figure 6b shows the effects of an algorithm that errs in the mixing state and simultaneously omits aerosol hygroscopicity. In this case, depending on RH and θ , $\tau(\text{ext})/\tau(\text{int})$ varies from 0.64 to 0.80, resulting in an underestimate of 20% to 40% compared to the above

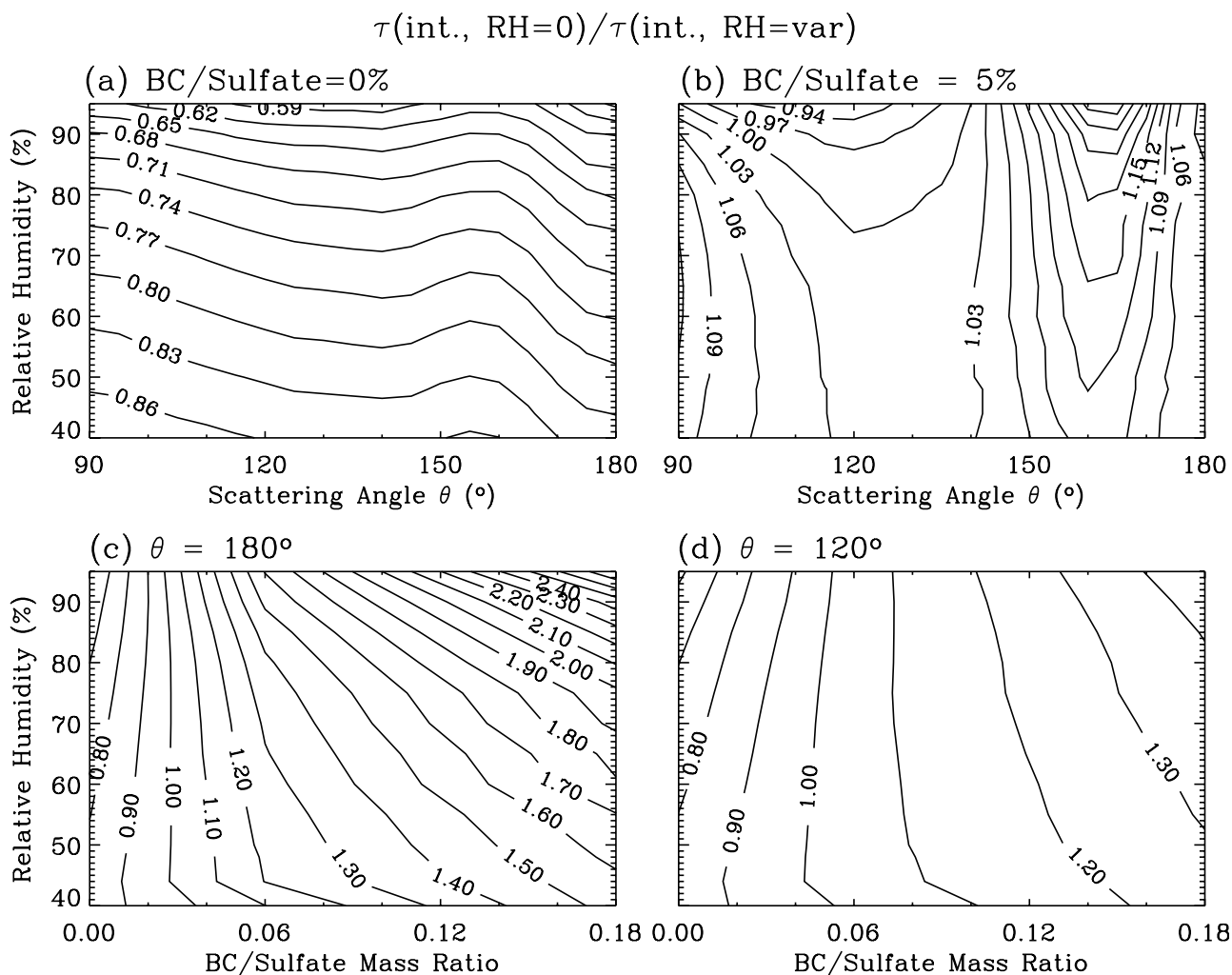


Figure 5. Isopleths of the ratio of retrieved aerosol optical thickness (τ) excluding aerosol hygroscopicity (i.e., $\text{RH} = 0$) to that including it. (a) Variable scattering angles (θ); BC/sulfate mass ratio of 0%. (b) Variable θ ; BC/sulfate mass ratio of 5%. (c) $\theta = 180^\circ$; variable BC/sulfate mass ratio. (d) $\theta = 120^\circ$; variable BC/sulfate mass ratio. Aerosol properties are given in Table 1. The INSO/(BC + sulfate + INSO) ratio is 35% for the calculations shown in this figure. The calculations are for a wavelength of $0.67 \mu\text{m}$, a solar zenith angle ($\cos^{-1} \mu_0$) of 30° , and ρ_{sfc} of 0.06. Black carbon and sulfate are internally mixed.

estimate of 2% to 20% for an algorithm including hygroscopicity. The underestimate increases because the omission of aerosol hygroscopicity in the algorithm omits the strong decrease of $P(\theta)$ for increasing RH (Figure 2b). The study at 180° isolates the effects of changes in $P(\theta)$ from those in ω (Figure 6d). The saturation effect in Figure 6d for increasing BC/sulfate mass ratio reflects the saturation of ω (Figure 3b).

[42] Figures 7a and 7b shows the ratio of the retrieved τ when assuming external mixing at 70% RH (as sometimes done in retrieval algorithms) to that when assuming internal mixing and variable RH (i.e., $\tau(\text{ext}, \text{RH} = 70\%)/\tau(\text{int}, \text{RH} = \text{var})$), which in many cases is more realistic for actual atmospheric aerosols. For a BC/sulfate mass ratio of 5%, the ratio varies from 0.85 to 0.99 depending on RH and the scattering angle (Figure 7a), indicating an underestimate of up to 15%. The variation with BC/sulfate mass ratio of $\tau(\text{ext}, \text{RH} = 70\%)/\tau(\text{int}, \text{RH} = \text{var})$ at 180° (Figure 7b) is

similar to that of $\tau(\text{ext}, \text{RH} = \text{var})/\tau(\text{int}, \text{RH} = \text{var})$ (Figure 6c), because the difference between $P(\theta)$ at 40% RH or 90% RH and $P(\theta)$ at 70% RH is relatively small at $\theta = 180^\circ$. Figures 7b and 6c are then related by $\omega(\text{ext}, \text{RH} = 70\%)/\omega(\text{ext}, \text{RH} = \text{var})$. Similar to Figure 6c, Figure 7b showed that for a wide range of RH from 40% to 95%, $\tau(\text{ext}, \text{RH} = 70\%)/\tau(\text{int}, \text{RH} = \text{var})$ is less than unity when ambient BC/sulfate aerosols are greater than 3%, suggesting that current operational retrieval algorithms might systematically underestimate the optical thickness of urban aerosols. The underestimate can be as large as 40% to 65% at conditions of low RH and high BC/sulfate mass ratio (Figure 7b).

[43] Figures 7c and 7d explore the effect of ρ_{sfc} on $\tau(\text{ext})/\tau(\text{int})$ at 70% RH. Increasing ρ_{sfc} decreases $\tau(\text{ext})/\tau(\text{int})$ and thus leads to larger underestimates of retrieved τ . The explanation is that larger ρ_{sfc} progressively increases multiple scattering, thus amplifying $\omega(\text{ext})/\omega(\text{int})$ by some

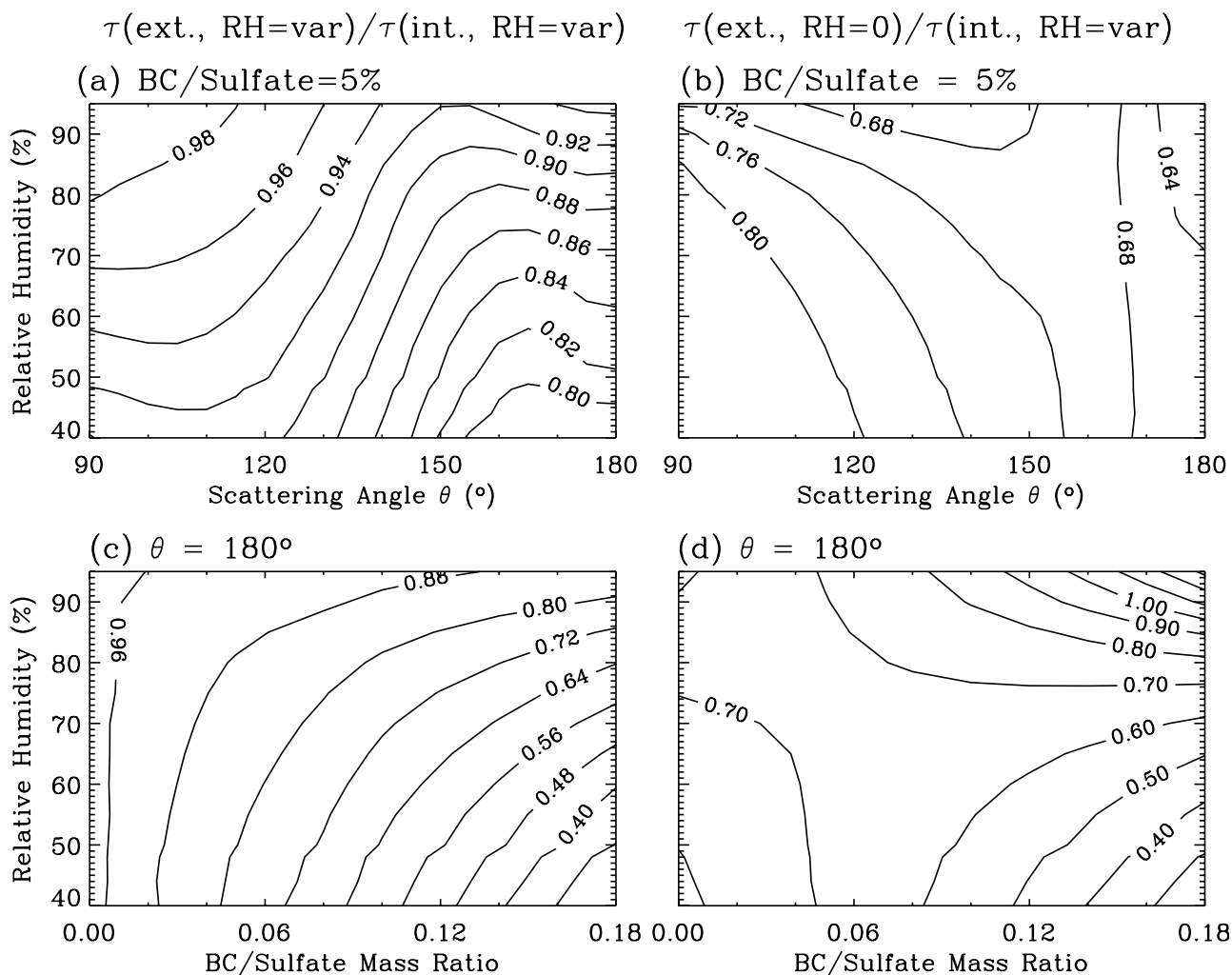


Figure 6. Isopleths of the ratio of the retrieved aerosol optical thickness (τ) assuming external mixing to that assuming internal mixing. (a) Hygroscopic growth included in the case of external mixing; variable scattering angles (θ); BC/sulfate mass ratio of 5%. (b) Hygroscopic growth excluded (i.e., RH = 0) in the case of external mixing; variable θ ; BC/sulfate mass ratio of 5%. (c) Hygroscopic growth included in the case of external mixing; $\theta = 180^\circ$; variable BC/sulfate mass ratio. (d) Hygroscopic growth excluded (i.e., RH = 0) in the case of external mixing; backscattering angle of 180° ; variable BC/sulfate mass ratio. Aerosol properties are given in Table 1. The INSO/(BC + sulfate + INSO) ratio is 35% for the calculations shown in this figure. The calculations are for a wavelength of $0.67 \mu\text{m}$, a solar zenith angle ($\cos^{-1} \mu_0$) of 30° , and ρ_{sfc} of 0.06.

exponential factor above unity and decreasing $\tau(\text{ext})/\tau(\text{int})$. In effect, the cross cut of values at 70% RH in Figure 6a are increased for $\rho_{sfc} < 0.06$ in Figure 7c and correspondingly decreased for $\rho_{sfc} > 0.06$. A second countervailing effect is the decreasing impact for increasing ρ_{sfc} of differences between down- and up-scattering (i.e., the role of $P(\theta)$), thereby increasing $\tau(\text{ext})/\tau(\text{int})$ for the reasons discussed in relation to Figure 6a. Nevertheless, the results in Figure 7c show that this second effect is quantitatively less important than the role of the single-scattering albedo.

[44] The dependence of $\tau(\text{ext})/\tau(\text{int})$ on ρ_{sfc} or BC/sulfate mass ratio is shown in Figure 7d for $\theta = 180^\circ$ and 70% RH. The retrieved τ is underestimated at 70% RH throughout the parameter range shown in the figure. Moreover, retrieval errors of 100% are possible for BC/sulfate mass ratios greater than 0.12 and $0.06 < \rho_{sfc} < 0.10$. In agreement with

Figure 6c at 70% RH, consideration of BC/sulfate mixing state is progressively more important at higher mass ratios. Surface reflectances greater than 0.1 or BC/sulfate mass ratios larger than 5% further increase the retrieval bias, including the possibility of unphysical retrievals (Figure 7d). Hence cautions are needed in use of current operational retrieval algorithms in the developing countries (such in Indian) where the single scattering albedo of urban aerosol can be as low as 0.78 with BC mass ratios larger than 10% [Ganguly *et al.*, 2006].

3.2.3. Uncertainties in Aerosol Effective Radius

3.2.3.1. Effect of Hygroscopicity

[45] The effects of aerosol hygroscopicity on the Angstrom exponent and the aerosol effective radius are shown in Figure 8 for the cases of external and internal mixing of BC and sulfate, in the absence of INSO particles. Sulfate

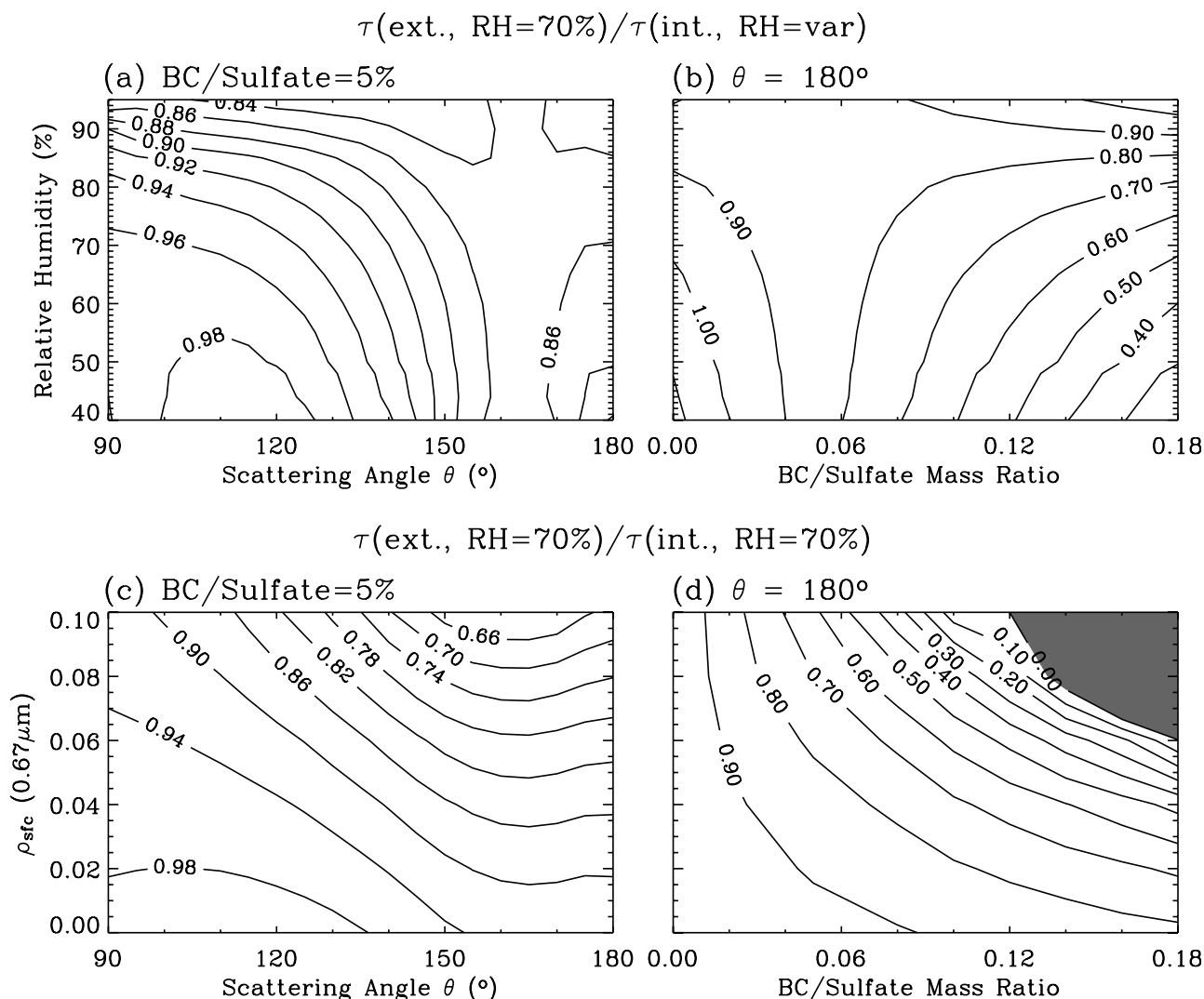


Figure 7. Isoleths of the ratio of the retrieved aerosol optical thickness (τ) assuming external mixing with optical properties at 70% RH to that assuming internal mixing with optical properties at either 70% RH or variable with RH. (a) Optical properties of variable RH in the case of internal mixing; variable scattering angle θ ; BC/sulfate mass ratio of 5%. (b) Optical properties of variable RH in the case of internal mixing; $\theta = 180^\circ$; variable BC/sulfate mass ratio. (c) Optical properties at 70% RH in the case of internal mixing; variable θ ; BC/sulfate mass ratio of 5%; shown for increasing surface reflectance. (d) Optical properties at 70% RH in the case of internal mixing $\theta = 180^\circ$; variable BC/sulfate mass ratio; shown for increasing surface reflectance. Aerosol properties are given in Table 1. The INSO/(BC + sulfate + INSO) ratio is 35% for the calculations shown in this figure. The calculations are for a wavelength of $0.67 \mu\text{m}$, a solar zenith angle ($\cos^{-1} \mu_0$) of 30° , and ρ_{sfc} of 0.06 (Figures 7a and 7b). In the shaded region of Figure 7d, $\rho_{\text{model_toa}}$ associated with $\tau(\text{int., RH} = 70\%)$ can be matched by $\tau(\text{ext., RH} = 70\%)$ only for negative values of the latter, which is physically unrealistic (see further in section 3.2.2).

hygroscopic growth at elevated RH increases r_{eff} and decreases α . Increasing RH from 50% to 90%, for example, increases r_{eff} by $0.1 \mu\text{m}$, regardless of the aerosol mixing state.

[46] The effects on r_{eff} and α of an increasing presence of externally mixed coarse-mode INSO aerosol particles, as defined by the INSO/(sulfate + BC) mass ratio, are shown in Figure 9. A growing presence of INSO increases r_{eff} and decreases α for all RH values, irrespective of the internal or external mixing state of BC and sulfate, and the magnitude of this effect is greater at lower RH than at elevated RH. For

instance, increasing the INSO/(sulfate + BC) mass ratio from 0.1 to 1.0 increases r_{eff} by $0.08 \mu\text{m}$ (Figure 9a) and decreases α by 0.1 (Figure 9b). The effects on r_{eff} and α decrease to $0.03 \mu\text{m}$ and 0.1, respectively, at 90% RH.

[47] The data in Figure 9 constitute examples of α and r_{eff} calculated for specific RH values, specific internal/external mixing states of BC and sulfate, specific BC-to-sulfate mass ratios of 5%, and specific INSO/(sulfate + BC) mass ratios. Therefore the functional relationship $r_{\text{eff}} = h(\alpha; \text{mixing state, RH, INSO}/(\text{sulfate} + \text{BC}) \text{ mass ratio})$ exists in these data. In Figure 10a, the effect of hygroscopicity is shown by

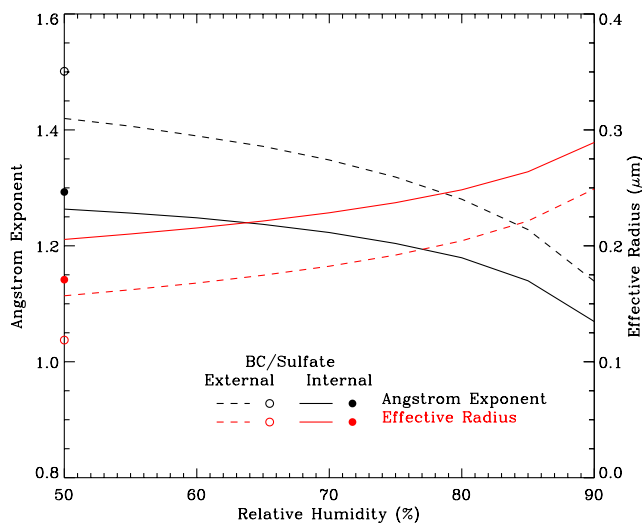


Figure 8. Angstrom exponent α and aerosol effective radius r_{eff} as a function of RH for the cases of internal and external mixing. The points show the values at 0% RH (i.e., disregard hygroscopicity). The α value is calculated based upon optical properties at 0.55 and 0.67 μm . The BC/sulfate mass ratio is 5%. Aerosol properties are given in Table 1. INSO particles are not included in the calculations.

the lines drawn for $r_{eff} = h(\alpha)$ at several RH values (namely, separate lines for 0%, 50%, 70%, 80%, and 90% RH) for external mixing of BC/sulfate. The INSO/(sulfate + BC) mass ratio runs from 1.0 at the start of each line to 0.1 at the end of each.

[48] A satellite observation α implies a retrieval of r_{eff} . Figure 10a for external mixing shows that a satellite algorithm omitting aerosol hygroscopicity (i.e., $r_{eff} = h(\alpha; \text{RH} = 0\%)$) greatly overestimates r_{eff} if the actual atmospheric RH is elevated. Specifically, at 90% compared to 0% RH, r_{eff} decreases by 0.1 to 0.4 μm depending on α . Maximum likelihood values of α of urban aerosols and of RH in urban regions are 1.3 and 70% [Dubovik *et al.*, 2002], respectively. These values imply a typical overestimate in r_{eff} of 0.20 μm when not accounting for aerosol hygroscopicity. A similar analysis for the case of internal mixing (Figure 10b) yields an overestimate in r_{eff} of 0.18 μm . These overestimates increase for atmospheric RH above 70% and for α values above 1.3 and vice versa for lower values of RH or α . Figures 10a and 10b therefore clearly show that a retrieval algorithm that entirely omits aerosol hygroscopicity results in a retrieved r_{eff} systematically larger than the true value, at least for aerosols having the properties given in Table 1.

[49] In comparison, a retrieval algorithm that uses the optical properties of an aerosol at 70% RH may overestimate or underestimate r_{eff} , depending on the actual RH of the atmosphere. For example, for an observed α of 1.3, the error in r_{eff} may be either negative by up to 0.15 μm or positive by up to 0.2 μm depending on whether the real atmospheric RH is below or above 70% RH, respectively (Figure 10a).

3.2.3.2. Effects of Aerosol Mixing State

[50] External or internal mixing has an important effect on the calculated relationship between the aerosol effective radius and the Angstrom exponent for fixed RH. For example, Figure 8 shows that at 70% RH the α and r_{eff} values are 1.35 and 0.17 μm , respectively, for external

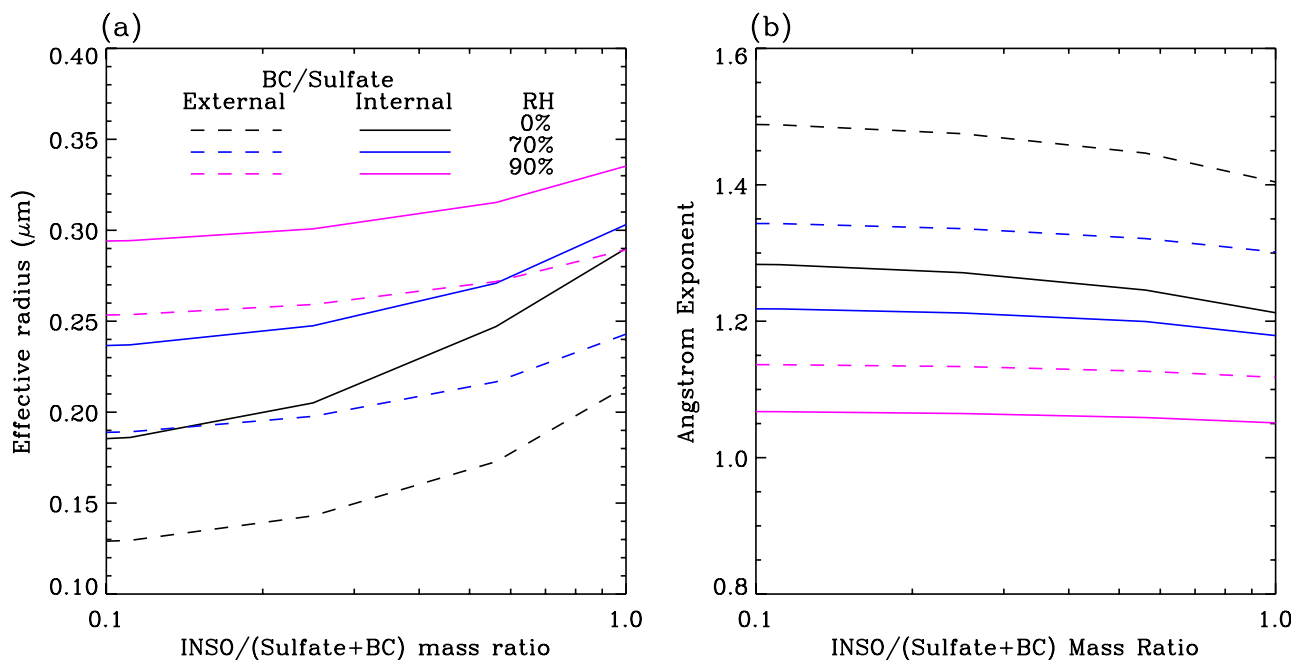


Figure 9. Effect of INSO/(sulfate+BC) mass ratio on (a) the aerosol effective radius and (b) the Angstrom exponent. Cases are shown for internal and external mixing and for 0% (i.e., disregard hygroscopicity), 70%, and 90% RH. The α value is calculated based upon optical properties at 0.55 and 0.67 μm . The BC/sulfate mass ratio is 5%. Aerosol properties are given in Table 1.

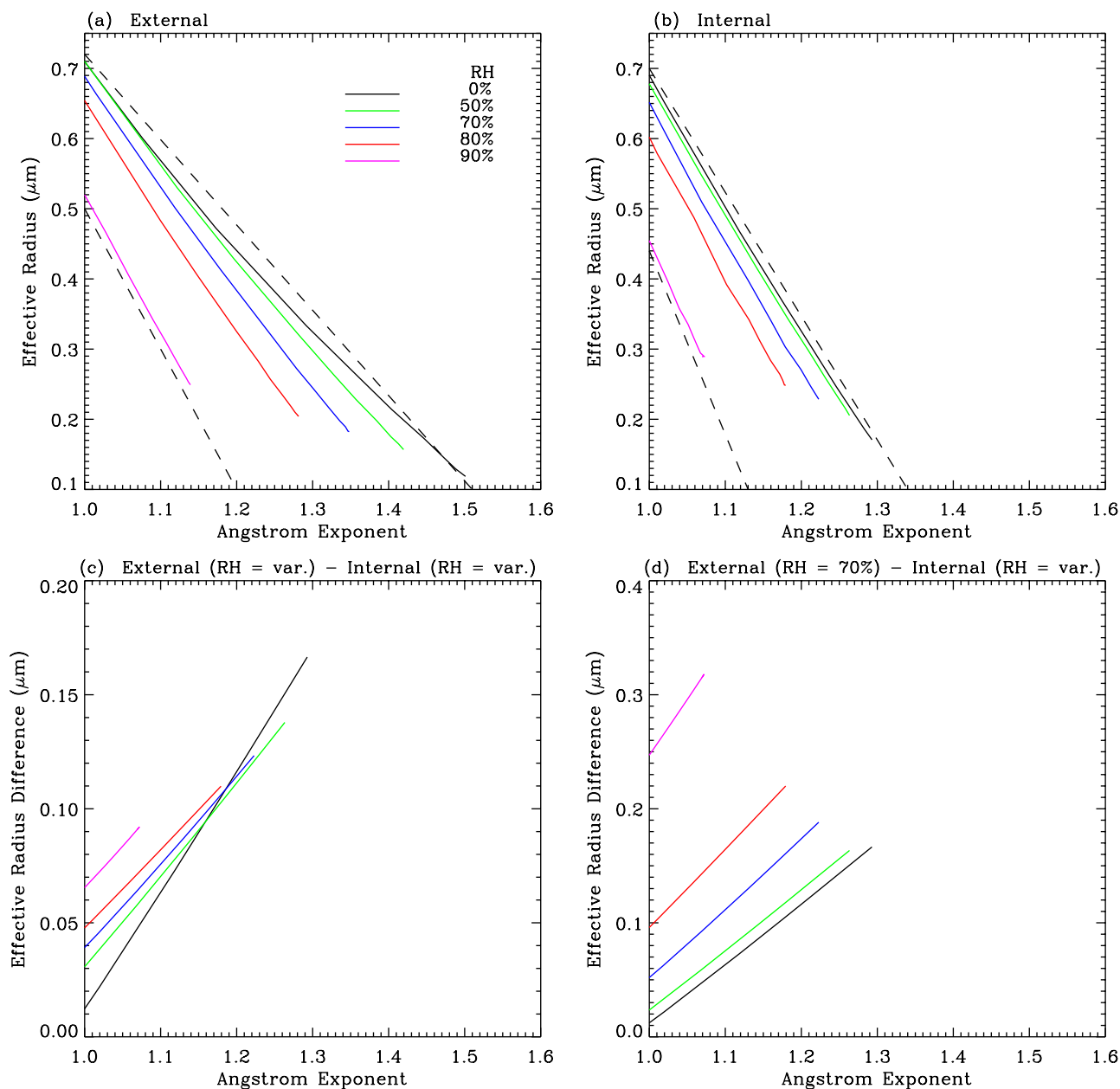


Figure 10. (a) Lines of $r_{eff} = h(\alpha)$; mixing: external BC/sulfate, RH:constant, INSO/(sulfate + BC) mass ratio:variable) for several RH values. The INSO/(sulfate + BC) mass ratio decreases from 1.0 to 0.1 along each line (see text). The dotted lines are drawn for $r_{eff} = 1.9 - 1.2\alpha$ at 0% RH and $r_{eff} = 2.5 - 2.0\alpha$ at 90% RH. (b) Same as panel a except that BC and sulfate are internally mixed. The dotted lines are drawn at $r_{eff} = 2.5 - 1.8\alpha$ for 0% RH (i.e., disregard hygroscopicity) and $r_{eff} = 3.4 - 2.9\alpha$ at 90% RH. (c) Difference plots for each pair of RH lines shown in Figures 10a and 10b, showing the effects of external compared to internal mixing. (d) Difference plots of the 70% RH line for external mixing compared to those of the variable RH lines for internal mixing. (The α value is calculated based upon optical properties at 0.55 and 0.67 μm . The BC/sulfate mass ratio is 5%. Aerosol properties are given in Table 1.)

mixing but change to 1.22 and 0.27 μm for internal mixing. These differences associated with external and internal mixing have two contributing factors. (1) The number concentration of aerosol particles is greater for external compared to internal mixing (cf. Appendix B). In particular, the BC mode at small size is eliminated upon internal mixing, thereby increasing r_{eff} and decreasing α , (2) Com-

pared to externally mixed particles, the core-shell microstructure of internally mixed BC/sulfate particles enhances absorption, thus reducing the wavelength dependence of K_{ext} and thereby decreasing α . Since this effect is purely optical, r_{eff} remains unchanged. Through a sensitivity analysis (not shown), we find that the first contribution is the primary factor behind the dependence of the α values on

mixing state. An implication of this finding in regard to satellite retrievals is that internal or external mixing assumptions in retrieval algorithms affect the inferred atmospheric aerosol number concentration, which can be a relevant quantity for follow-on applications such as predicting aerosol indirect effects on cloud formation [Charlson *et al.*, 1992].

[51] The effect of coarse-mode INSO when externally mixed with BC/sulfate is to decrease α and increase r_{eff} (Figure 9). For internally compared to externally mixed BC/sulfate (i.e., INSO externally mixed with BC and sulfate in both cases), internal mixing gives a larger r_{eff} and a smaller α (Figures 9a and 9b), which is consistent with the results shown in Figure 6. At 0% RH, the difference in α value calculated for internal compared to external mixing is approximately 0.2 across an INSO mass ratio range of 0.1 to 1.0 (Figure 9b). At 70% RH, across the same INSO range, the difference caused by mixing state is approximately 0.13. The decrease of the difference in α as RH increases occurs because the large sulfate particles at elevated RH have a weaker wavelength dependence of K_{ext} and thus there is a reduced effect of mixing.

[52] The effect of an assumed mixing state on the r_{eff} value retrieved by a satellite algorithm based upon the α value observed by the satellite sensors is shown in Figure 10c. At 0% RH, the difference in the retrieved r_{eff} for an assumption of external compared to internal mixing ranges from 0.01 to 0.17 μm as α varies from 1.0 to 1.3. At 70% RH, the difference range decreases to 0.04 to 0.14 μm across the same α range. For comparison, the effect of the assumption by a satellite retrieval algorithm of external mixing at 70% RH compared to internal mixing at variable RH (i.e., assumed atmospheric conditions) is shown in Figure 10d. At 0% RH, the change in r_{eff} for assuming external mixing ranges from 0.01 to 0.16 μm as α varies from 1.0 to 1.3. At 70% RH, the difference increases to 0.05 to 0.25 μm across the same α range.

4. Conclusions

[53] Reducing uncertainties in satellite retrievals of urban aerosols is an important goal because satellite-based aerosol products are making valuable contributions to monitoring and ameliorating a diverse array of problems, such as air quality monitoring [Al-Saadi *et al.*, 2005], initializing and validating regional and global aerosol models [Wang *et al.*, 2004], and quantifying aerosol radiative forcing [Kaufman *et al.*, 2002]. Theoretical simulation of retrievals is a valuable tool for assessing uncertainties [Mishchenko and Travis, 1997; Yan *et al.*, 2002; Masuda *et al.*, 2002], even the more so because of interfering uncertainties in real applications [Wang *et al.*, 2003a]. The goal of reaching the same confidence level regarding aerosol forcing as regarding greenhouse gases requires an accuracy of satellite-derived τ of 0.01 or less [Chylek *et al.*, 2003]. On the basis of our current study, this goal cannot be successfully achieved without a proper treatment of aerosol hygroscopicity and aerosol mixing state in retrieval algorithms, at least as applied to urban aerosols.

[54] The results reported herein show that the single-scattering albedo of urban aerosols is sensitive to the BC/sulfate mixing state, which is consistent with Ackerman and

Toon [1981]. More interestingly, we find that the assumptions regarding the BC/sulfate mixing state significantly impact the $r_{eff} = h(\alpha)$ relationship. This important finding has been overlooked in previous studies. Although the impact of BC/sulfate mixing state becomes less important as RH increases, the effects of aerosol hygroscopicity on the aerosol phase function and aerosol single-scattering albedo correspondingly increase.

[55] The present study further evaluates the possible uncertainties in the satellite retrieval of τ and r_{eff} if treatments of aerosol hygroscopicity and aerosol mixing state are omitted from the algorithm. For the most favorable case of surface reflectance less than 0.1 and internally mixed BC/sulfate mass ratio less than 2%, a retrieval algorithm assuming that aerosols are externally mixed at 70% RH lead to an uncertainty in τ of as small as 10%. The uncertainty becomes a systematic underestimate if BC/sulfate ratio is larger than 3%. For typical cases of urban aerosols having BC/sulfate internally mixed at mass ratios of 5%, an algorithm that assumes aerosol optical properties of 0% RH results in up to a 50% underestimate of τ and an uncertainty of $\pm 0.2 \mu\text{m}$ for r_{eff} depending on ambient RH. In comparison, for the case of aerosol optical properties fixed at 70% RH in the retrieval algorithm, the errors in τ and r_{eff} are 40% and $\pm 0.1 \mu\text{m}$, respectively. For the most unfavorable case of surface reflectance greater than 0.1 or BC/sulfate mass ratio larger than 5%, the retrieval bias, including the possibility of unphysical retrievals, increases further.

[56] The practical retrieval of τ and r_{eff} can be affected by many factors in addition to those analyzed in this paper, such as the characterization of surface reflectance, the sensor calibration, and the vertical distribution of aerosols. The impact of the first two factors on retrieval accuracy is analyzed by Wang *et al.* [2003a]; in the present study, we further show that ρ_{sfc} values exceeding the dark-surface condition can result in an underestimate of the aerosol optical thickness of absorbing urban aerosols. The retrieval uncertainties caused by the multilayer aerosol distribution, possibly due to long-range aerosol transport and causing vertical variation of aerosol optical properties, are not assessed in the present study because our treatment assumes that aerosols are well mixed in the boundary layer. We make this assumption because turbulent mixing in cloud-free days is usually strong for the observation schedule of polar-orbiting satellites, i.e., from local late morning (e.g., 10:30 for Terra) to local early afternoon (e.g., 13:30 for Aqua [Wang and Christopher, 2003]). Hence the results of this study should be further tested by using actual retrieval algorithms and satellite data in conjunction with simultaneous and accurate ground-based measurements of surface reflectance, ambient relative humidity, particle composition and microstructure, and aerosol optical properties.

[57] Compared to other aerosol types, the heterogeneity in urban-aerosol optical properties is large and therefore poses a challenge for successful satellite applications. The heterogeneity of urban aerosols arises from the different industrial and seasonal patterns of aerosols around the world. Therefore although detailed information of aerosol chemical composition cannot realistically be available for routine retrievals, we suggest that, as a step forward, the relative mass ratios of sulfate particles, soot, and INSO should be included in the retrieval algorithm for the correct

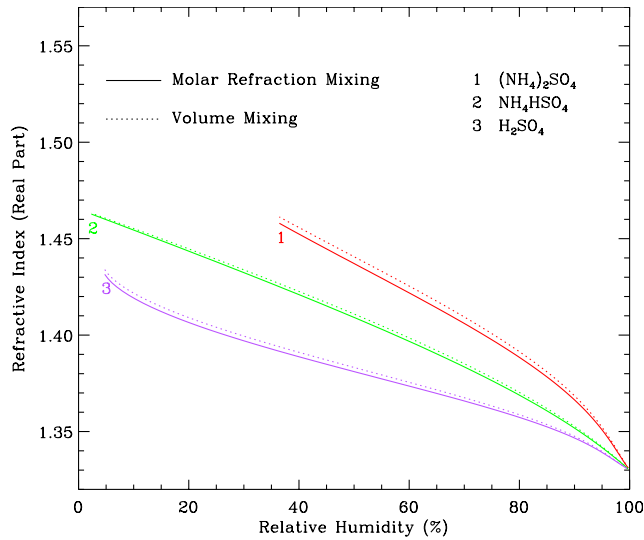


Figure A1. Real part of refractive index for aqueous solutions of ammonium sulfate, ammonium bisulfate, and sulfuric acid at different relative humidities. Values are calculated by using a volume-mixing rule (dotted line) and a molar-refraction rule (solid line). The refractive indices at 0% RH (dry conditions) are from *Tang and Munkelwitz* [1994] and *Tang* [1996]. The line for aqueous ammonium sulfate begins at the CRH value of 35%.

selection of aerosol optical model. In this regard, we recommend the use of chemical transport models (CTMs) to provide such information for the satellite retrieval of aerosols. CTM simulations, even with their uncertainties, are able to capture the large scale features of aerosol composition, distribution, and to a limited extent the aerosol phase and aerosol mixing state [*Jacobson, 2001; Park et al., 2004; Martin et al., 2004*], thus providing valuable information for selection of the proper aerosol optical models in the retrievals. This approach is similar to the currently implemented retrieval algorithms for trace gases from satellite observations, such as CO retrievals from the MOPITT satellite for which CTM-based trace gas profiles are used as a first guess in the retrieval algorithm [*Pan et al., 1998*]. Therefore in addition to the needs for improvements in sensor calibration, surface reflectance characterization, and cloud screening, incorporation of aerosol information from CTMs is recommended for a better consideration of aerosol hygroscopicity and aerosol mixing state and, thereby, for improvements in the accuracies of satellite retrievals of τ and r_{eff} for urban aerosols.

Appendix A: Refractive Index: Volume-Mixing and Molar Refraction Rules

[58] The volume-mixing rule calculates the effective refractive index (m) of a mixture as the sum of the refractive index (m_j) of each component j weighted by its corresponding volume fraction (V_j), i.e., $m = \sum V_j m_j$ [*Heller, 1945*]. This mixing rule is used in the several widely employed databases of aerosol optical properties [*Shettle and Fenn, 1979; d'Almeida et al., 1991; Hess et al., 1998*]. The molar-refraction rule infers the effective refractive

index from the molar refractions (R), which is calculated as the sum of the component molar refractions (R_j) weighted by the corresponding mole fractions (x_j), i.e., $R = \sum x_j R_j$ [*Moelwyn-Hughes, 1961; Stelson and Seinfeld, 1982; Tang, 1996*]. The molar refraction is then as follows: $R = V_m(m^2 - 1)/(m^2 + 1)$, where V_m is the molar volume. Figure A1 shows that these two mixing rules yield similar results for the effective refractive index of aqueous aerosols of ammonium sulfate, ammonium hydrate sulfate, and sulfuric acid.

Appendix B: Internal or External Mixing: Mass Conservation and the Calculation of Core-to-Shell Radius Ratio

[59] An explanation of how the internal and external mixing calculations are performed is necessary to completely understand the effects of mixing on the aerosol optical properties shown in Figures 2 through 10. The mass mixing ratio M_j of each aerosol type is conserved. An associated implication is that the volume mixing ratio V_j of each aerosol type is also conserved because the chemical species j are immiscible with one another. A further implication is that total aerosol number concentration decreases from $(N_{BC} + N_{sulf} + N_{INSO})$ for external mixing to $(N_{BC/sulf} + N_{INSO})$ for internal mixing because $N_{BC/sulf}$ is set equal to N_{sulf} . As a result, even before consideration of any other factors, K^{ext} and K^{sca} decrease in the calculations for internal compared to external mixing because of the lower number concentration of the former, even though the sulfate particle size increases slightly.

[60] The number size distributions for external mixing are defined by the r_g and σ_g parameters given in Table 1, equation (1) in the main text, and N_j values for prescribed mass ratios. In further regard to N_j , the mass mixing ratio is given by the Hatch-Choate relations for a log-normal size distribution as follows:

$$M_j = \frac{4\pi}{3} \eta_j \int r^3 n_j(r) dr = \frac{4\pi}{3} N_j \eta_j r_{g,j}^3 \exp(4.5 \ln^2 \sigma_{g,j}) \quad (B1)$$

where η is the particle density. Equation (B1) combined with the parameters in Table 1 is sufficient to define the number size distribution of an externally mixed aerosol having, for example, 5% by mass BC and 95% by sulfate (e.g., Figure 2c). Similarly, the running axis of Figure 9 of the mass ratio of INSO/(sulfate + BC) is defined by equation (B1) and Table 1 for an externally mixed aerosol.

[61] For internal mixing, the BC particles are modeled as imbedded in the sulfate particles, thereby increasing $r_{g,sulf}$ of external mixing by some multiplicative factor γ to a value $r_{g,BC/sulf}$ of internal mixing, namely $r_{g,BC/sulf} \equiv \gamma r_{g,sulf}$. Given that the integrated particle volume is conserved regardless of internal or external mixing (i.e., $V_{internal} = V_{external}$), setting $\sigma_{g,BC/sulf} = \sigma_{g,sulf}$ and using $V_j = M_j/\rho_j$, we derive the value of the factor γ , as follows:

$$V_{BC/sulf} = N_{sulf} \gamma^3 r_{g,sulf}^3 \exp(4.5 \ln^2 \sigma_{g,sulf}) = \gamma^3 V_{sulf} \quad (B2)$$

$$V_{BC/sulf} = V_{internal} = V_{external} = V_{BC} + V_{sulf} \quad (B3)$$

Combining equations (B2) and (B3) yields:

$$\gamma = \left(1 + \frac{V_{BC}}{V_{sulf}}\right)^{1/3} \quad (\text{B4})$$

where V_{BC} and V_{sulf} are defined by the parameters of external mixing (e.g., 5% BC/sulfate mass) and used in the calculation of γ for internal mixing. Figure 2b compared to Figure 2c provides an example of this approach in use.

[62] The γ value is an important input to the shell/core optical model used to calculate the effects of BC/sulfate internal mixing on the aerosol optical properties. For V_{BC} and V_{sulf} defined by the parameters r_g and σ_g of Table 1, the γ value at low RH does not exceed 1.007 for many cases in this study, namely those having BC compared to sulfate of 20% or less by mass. The corresponding upper limit of the core-to-shell ratio is 0.27. The γ value and the corresponding core-to-shell ratio decrease further at elevated RH because of hygroscopic growth by sulfate.

[63] **Acknowledgments.** We are grateful for support received from the NSF Atmospheric Chemistry Program (ATM-0317583). J. Wang is supported by a NOAA Climate & Global Change Postdoctoral Fellowship under the administration of the UCAR visiting scientist program. The authors thank D. J. Jacob for insightful discussion and W. Wiscombe for computer codes.

References

- Abdou, W. A., D. J. Diner, J. V. Martonchik, C. J. Bruegge, R. A. Kahn, B. J. Gaitley, J. A. Breaun, L. A. Remer, and B. Holben (2005), Comparison of coincident Multiangle Imaging Spectroradiometer and Moderate Resolution Imaging Spectroradiometer aerosol optical depths over land and ocean scenes containing Aerosol Robotic Network sites, *J. Geophys. Res.*, *110*, D10S07, doi:10.1029/2004JD004693.
- Ackerman, T., and O. B. Toon (1981), Absorption of visible radiation in atmosphere containing mixtures of absorbing and non-absorbing particles, *Appl. Opt.*, *20*, 3661–3668.
- Al-Saadi, J., et al. (2005), Improving national air quality forecasts with satellite aerosol observations, *Bull. Am. Meteorol. Soc.*, *86*, 1249–1261.
- Castanho, A. D., J. V. Martins, P. V. Hobbs, P. Artaxo, L. Remer, M. Yamasoe, and P. R. Colarco (2005), Chemical characterization of aerosols on the east coast of the United States using aircraft and ground-based stations during the CLAMS experiment, *J. Atmos. Sci.*, *62*, 934–946.
- Charlson, R. J., S. E. Schwartz, J. M. Hales, R. D. Cess, J. A. Coakley, J. E. Hansen, and D. J. Hoffman (1992), Climate forcing by anthropogenic aerosols, *Science*, *255*, 423–430.
- Chu, D. A., Y. J. Kaufman, G. Zibordi, J. D. Chern, J. Mao, C. Li, and B. N. Holben (2003), Global monitoring of air pollution over land from the Earth Observing System-Terra Moderate Resolution Imaging Spectroradiometer (MODIS), *J. Geophys. Res.*, *108*(D21), 4661, doi:10.1029/2002JD003179.
- Chylek, P., G. Videen, D. Ngo, R. G. Pinnick, and J. D. Klett (1995), Effect of black carbon on the optical properties and climate forcing of sulfate aerosols, *J. Geophys. Res.*, *100*(D8), 16,325–16,332.
- Chylek, P., B. Henderson, and M. Mishchenko (2003), Aerosol radiative forcing and the accuracy of satellite aerosol optical depth retrieval, *J. Geophys. Res.*, *108*(D24), 4764, doi:10.1029/2003JD004044.
- d'Almeida, G. A., P. Koepke, and E. P. Shettle (1991), *Atmospheric Aerosols: Global Climatology and Radiative Characteristics*, 561 pp., A. Deepak, Hampton, Va.
- Deuze, J. L., M. Herman, P. Boloube, and D. Tanre (1999), Characterization of aerosols over ocean from POLDER/ADEOS-1, *Geophys. Res. Lett.*, *26*, 1421–1424.
- Dubovik, O., B. Holben, T. F. Eck, A. Smimov, Y. J. Kaufman, M. D. King, D. Tanre, and I. Slutsker (2002), Variability of absorption and optical properties of key aerosol types observed in worldwide locations, *J. Atmos. Sci.*, *59*, 590–608.
- Eck, T. F., B. N. Holben, J. S. Reid, O. Dubovik, A. Smimov, N. T. O'Neill, I. Slutsker, and S. Kinne (1999), Wavelength dependence of the optical depth of biomass burning, urban, and desert dust aerosols, *J. Geophys. Res.*, *104*, 31,333–31,349.
- Engel-Cox, J. A., C. H. Holloman, B. W. Coutant, and R. M. Hoff (2004), Qualitative and quantitative evaluation of MODIS satellite sensor data for regional and urban scale air quality, *Atmos. Environ.*, *38*, 2495–2509.
- Ferrare, R., R. S. Fraser, and Y. J. Kaufman (1990), Satellite measurements of large-scale air pollution: Measurements of forest fire smoke, *J. Geophys. Res.*, *95*, 9911–9925.
- Ganguly, D., A. Jayaraman, and H. Gadhavi (2006), Physical and optical properties of aerosols over an urban location in western India: Seasonal variabilities, *J. Geophys. Res.*, *111*, D24206, doi:10.1029/2006JD007392.
- Hanel, G. (1976), The properties of atmospheric aerosol particles as functions of the relative humidity at thermodynamic equilibrium with the surrounding moist air, *Adv. Geophys.*, *19*, 72–188.
- Hansen, J. E., and L. D. Travis (1974), Light scattering in planetary atmospheres, *Space Sci. Rev.*, *16*, 527–610.
- Heller, W. (1945), The determination of refractive index of colloidal particles by means of a new mixture rule or from measurements of light scattering, *Phys. Rev.*, *68*, 5–10.
- Hess, M., P. Koepke, and I. Schult (1998), Optical properties of aerosols and clouds: The software package OPAC, *Bull. Am. Meteorol. Soc.*, *79*, 831–844.
- Higurashi, A., and T. Nakajima (1999), Development of a two-channel aerosol retrieval algorithm on a global scale using NOAA AVHRR, *J. Atmos. Sci.*, *56*, 924–941.
- Ignatov, A. M., and L. L. Stowe (2000), Physical basis, premise, and self-consistency of aerosol retrievals from TRMM VIRS, *J. Appl. Meteorol.*, *39*, 2257–2277.
- Jacobson, M. Z. (2001), Strong radiative heating due to the mixing state of black carbon in atmospheric aerosols, *Nature*, *409*, 695–697.
- Johnson, K. S., B. Zuberi, L. T. Molina, M. J. Molina, M. J. Iedema, J. P. Cowin, D. J. Gaspar, C. Wang, and A. Laskin (2005), Processing of soot in an urban environment: Case study from the Mexico City metropolitan area, *Atmos. Chem. Phys.*, *5*, 3033–3043.
- Kahn, R., B. J. Gaitley, J. V. Martonchik, D. J. Diner, K. A. Crean, and B. Holben (2005a), MISR global aerosol optical depth validation based on two years of coincident AERONET observations, *J. Geophys. Res.*, *110*, D10S04, doi:10.1029/2004JD004706.
- Kahn, R., et al. (2005b), MISR Calibration and implications for low-light-level aerosol retrieval over dark water, *J. Atmos. Sci.*, *62*, 1032–1052.
- Kaufman, Y. J., D. Tanre, H. R. Gordon, T. Nakajima, J. Lenoble, R. Frouin, H. Grassl, B. M. Herman, M. D. King, and P. M. Teillet (1997), Passive remote sensing of tropospheric aerosol and atmospheric correction for the aerosol effect, *J. Geophys. Res.*, *102*, 16,815–16,830.
- Kaufman, Y. J., D. Tanre, and O. Boucher (2002), A satellite view of aerosols in climate systems, *Nature*, *419*, 215–223.
- Kaufman, Y. J., et al. (2005), A critical examination of the residual cloud contamination and diurnal sampling effects on MODIS estimates of aerosol over ocean, *IEEE Trans. Geosci. Remote Sens.*, *43*, 2886–2897.
- King, M. D., Y. J. Kaufman, D. Tanre, and T. Nakajima (1999), Remote sensing of tropospheric aerosols from space: Past, present, and future, *Bull. Am. Meteorol. Soc.*, *80*, 2229–2259.
- Lesins, G., P. Chylek, and U. Lohmann (2002), A study of internal and external mixing scenarios and its effect on aerosol optical properties and direct radiative forcing, *J. Geophys. Res.*, *107*(D10), 4094, doi:10.1029/2001JD000973.
- Levy, R. C., L. A. Remer, and Y. J. Kaufman (2004), Effects of neglecting polarization on the MODIS aerosol retrieval over land, *IEEE Trans. Geosci. Remote Sens.*, *42*, 2576–2583.
- Li, J., J. G. D. Wong, J. S. Dobbie, and P. Chylek (2001), Parameterization of the optical properties of sulfate aerosols, *J. Atmos. Sci.*, *58*, 193–209.
- Liou, K. N. (2002), *An Introduction to Atmospheric Radiation*, 583 pp., Elsevier, New York.
- Liu, Y., R. J. Park, D. J. Jacob, Q. Li, V. Kilaru, and J. A. Sarmat (2004), Mapping annual mean ground-level PM 2.5 concentrations using Multi-angle Imaging Spectroradiometer aerosol optical thickness over the contiguous United States, *J. Geophys. Res.*, *109*, D22206, doi:10.1029/2004JD005025.
- Martin, S. T. (2000), Phase transitions of aqueous atmospheric particles, *Chem. Rev.*, *100*, 3403–3453.
- Martin, S. T., H. M. Hung, R. J. Park, D. J. Jacob, R. J. D. Spurr, K. V. Chance, and M. Chin (2004), Effects of the physical state of tropospheric ammonium-sulfate-nitrate particles on global aerosol direct radiative forcing, *Atmos. Chem. Phys.*, *4*, 183–214.
- Martonchik, J. V., D. J. Diner, R. A. Kahn, T. P. Ackerman, M. M. Verstraete, B. Pinty, and H. R. Gordon (1998), Techniques for the retrieval of aerosol properties over land and ocean using multiangle imaging, *IEEE Trans. Geosci. Remote Sens.*, *36*, 1212–1227.
- Masuda, K., H. Ishimoto, and T. Takashima (2002), Dependence of the spectral aerosol optical thickness retrieval from space on measurement errors and model assumptions, *Int. J. Remote Sens.*, *23*, 3835–3851.

- McClatchey, R. A., R. W. Fenn, J. E. A. Selby, F. E. Volz, and J. S. Garing (1971), Optical properties of the atmosphere, *Rep. AFCRL-TR-71-0279*, *Environ. Res. Pap.* 354, Air Force Cambridge Res. Lab., Bedford, Mass.
- Mishchenko, M. I., and L. D. Travis (1997), Satellite retrieval of aerosol properties over the ocean using polarization as well as intensity of reflected sunlight, *J. Geophys. Res.*, 102, 16,989–17,013.
- Mishchenko, M. I., I. V. Geogdzhayev, B. Cairns, W. B. Rossow, and A. A. Lacis (1999), Aerosol retrievals over the ocean by use of channels 1 and 2 AVHRR data: Sensitivity analysis and preliminary results, *Appl. Opt.*, 38, 7325–7341.
- Moelwyn-Hughes, E. A. (1961), *Physical Chemistry*, Elsevier, New York.
- Moulin, C., C. E. Lambert, F. Dulac, and U. Dayan (1997), Control of atmospheric export of dust from North Africa by the North Atlantic Oscillation, *Nature*, 387, 691–694.
- Nemesure, S., R. Wagener, and S. E. Schwartz (1995), Direct shortwave forcing of climate by the anthropogenic sulfate aerosol: Sensitivity to particle size, composition, and relative humidity, *J. Geophys. Res.*, 100, 26,105–26,116.
- Pan, L., J. C. Gille, D. P. Edwards, P. L. Bailey, and C. D. Rodgers (1998), Retrieval of tropospheric carbon monoxide for the MOPITT experiment, *J. Geophys. Res.*, 103, 32,277–32,290.
- Park, R. J., D. J. Jacob, B. D. Field, R. M. Yantosca, and M. Chin (2004), Natural and trans-boundary pollution influences on sulfate-nitrate-ammonium aerosols in the United States: Implications for policy, *J. Geophys. Res.*, 109, D15204, doi:10.1029/2003JD004473.
- Rao, C. R., L. L. Stowe, and P. McClain (1989), Remote sensing of aerosols over oceans using AVHRR data, theory, practice and application, *Int. J. Remote Sens.*, 10, 743–749.
- Redemann, J., P. B. Russell, and P. Hamill (2001), Dependence of aerosol light absorption and single-scattering albedo on ambient relative humidity for sulfate aerosols with black carbon cores, *J. Geophys. Res.*, 106, 27,485–27,495.
- Remer, L. A., et al. (2005), The MODIS aerosol algorithm, product, and validation, *J. Atmos. Sci.*, 62, 947–973.
- Ricchiazzi, P., S. Yang, C. Gautier, and D. Sowle (1998), SBDART: A research and teaching software tool for plane-parallel radiative transfer in the Earth's atmosphere, *Bull. Am. Meteorol. Soc.*, 79, 2101–2114.
- Schwarz, J. P., et al. (2006), Single-particle measurements of mid-latitude black carbon and light-scattering aerosols from the boundary layer to the lower stratosphere, *J. Geophys. Res.*, 111, D16207, doi:10.1029/2006JD007076.
- Shettle, E. P., and R. W. Fenn (1979), Models for the aerosols of the lower atmosphere and the effects of humidity variations on their optical properties, *Rep. no. AFGL-TR-79-0214*, *ERP No. 676*, Air Force Geophys. Lab., Optical Phys. Div., Hanscom Air Force Base, Mass.
- Stamnes, K., S.-C. Tsay, W. Wiscombe, and K. Jayaweera (1988), Numerically stable algorithm for discrete-ordinate-method radiative transfer in multiple scattering and emitting layered media, *Appl. Opt.*, 27, 2502–2509.
- Stelson, A. W., and J. H. Seinfeld (1982), Thermodynamic prediction of the water activity, NH_4NO_3 , dissociation constant, density and refractive index for the NH_4NO_3 - $(\text{NH}_4)_2\text{SO}_4$ - H_2O system at 25°C, *Atmos. Environ.*, 16, 2507–2514.
- Tang, I. N. (1996), Chemical and size effects of hygroscopic aerosols on light scattering coefficient, *J. Geophys. Res.*, 101, 19,245–19,250.
- Tang, I. N., and H. R. Munkelwitz (1994), Water activities, densities, and refractive indices of aqueous sulfates and sodium nitrate droplets of atmospheric importance, *J. Geophys. Res.*, 99, 18,801–18,808.
- Tanre, D., Y. J. Kaufman, M. Herman, and S. Matto (1997), Remote sensing of aerosol properties over oceans using the MODIS/EOS spectral radiance, *J. Geophys. Res.*, 102, 16,971–16,988.
- Tomasi, C., E. Caroli, and V. Vitale (1983), Study of the relationship between Angstrom's wavelength exponent and Junge particle size distribution exponent, *J. Clim. Appl. Meteorol.*, 22, 1707–1716.
- Wagener, R., S. Nemesure, and S. E. Schwartz (1997), Aerosol optical thickness over oceans: High space- and time-resolution retrieval and error-budget from satellite radiometry, *J. Appl. Meteorol.*, 14, 577–590.
- Wang, J., and S. A. Christopher (2003), Intercomparison between satellite-derived aerosol optical thickness and PM_{2.5} mass: Implications for air quality studies, *Geophys. Res. Lett.*, 30(21), 2095, doi:10.1029/2003GL018174.
- Wang, J., S. A. Christopher, J. S. Reid, H. Maring, D. Savoie, B. H. Holben, J. M. Livingston, P. B. Russell, and S. K. Yang (2003a), GOES 8 retrieval of dust aerosol optical thickness over the Atlantic Ocean during PRIDE, *J. Geophys. Res.*, 108(D19), 8595, doi:10.1029/2002JD002494.
- Wang, J., S. A. Christopher, F. Brechtel, J. Kim, B. Schmid, J. Redemann, P. B. Russell, P. Quinn, and B. N. Holben (2003b), Geostationary satellite retrievals of aerosol optical thickness during ACE-Asia, *J. Geophys. Res.*, 108(D23), 8657, doi:10.1029/2003JD003580.
- Wang, J., X. Liu, S. A. Christopher, J. S. Reid, E. A. Reid, and H. Maring (2003c), The effects of non-sphericity on geostationary satellite retrievals of dust aerosols, *Geophys. Res. Lett.*, 30(24), 2293, doi:10.1029/2003GL018697.
- Wang, J., U. Nair, and S. A. Christopher (2004), GOES-8 aerosol optical thickness assimilation in a mesoscale model: Online integration of aerosol radiative effects, *J. Geophys. Res.*, 109, D23203, doi:10.1029/2004JD004827.
- Wong, J., and Z. Li (2002), Retrieval of optical depth for heavy smoke aerosol plumes: Uncertainties and sensitivities to the optical properties, *J. Atmos. Sci.*, 59, 250–261.
- Yan, B., K. Stamnes, W. Li, B. Chen, J. J. Stamnes, and S.-C. Tsay (2002), Pitfalls in atmospheric correction of ocean color imagery: How should aerosol optical properties be computed?, *Appl. Opt.*, 41, 412–423.
- Zhang, K., W. Li, K. Stamnes, H. Eide, R. Spurr, and S. C. Tsay (2007), Assessment of the MODIS algorithm for retrieval of aerosol parameters over the ocean, *Appl. Opt.*, 46, 1525–1534.

S. T. Martin and J. Wang, Division of Engineering and Applied Science, Harvard University, 29 Oxford Street, Cambridge, MA 02138, USA. (scot_martin@harvard.edu; junwang@fas.harvard.edu)